Supporting Information

Photoinduced cation translocation in a molecular shuttle based on a calix[4]-biscrown including DCM and DMABN chromophores

N. Dozova,[a†] R. Kumar,[b†] T. Pradhan,[b] F. Lacombat,[a] B. Valeur,*[c] J. S. Kim,*[b] and P. Plaza*[a]

CONTENTS

1. Synthesis and characterization

General Materials and Methods: Chemicals were obtained from Aldrich, Alfa-Aesar, Acros Organics, TCI, and Carbosynth and used as received. Merck F254 TLC plates were used for checking reactions progress and silica gel 60 for column chromatography. $CDCl_3$ was used for checking ^1H and ^{13}C NMR spectra with TMS as an internal reference on Varian 300 and 400 MHz spectrometers. ESI-MS spectra were obtained using Thermo Scientific LTQ Orbitrap Mass Spectrometer. Compound **2** and **4** were synthesized according to literature procedures.[1]

*Compound **3**:* A mixture of calix[4]arene **1** (100 mg, 0.23 mmol) and Cs_2CO_3 (114 mg, 0.35 mmol) in dry CH_3CN was stirred for 30 min at room temperature. A solution of compound **2** in dry CH_3CN was added to the above mixture and refluxed for 40 hr. After completion of reaction, CH_3CN was evaporated and the reaction crude was extracted with methylene

chloride and water. The organic layer was dried over anhydrous $MgSO_4$, evaporated and purified by column (using ethyl acetate: hexane (1: 1)) to afford pure compound **3** (38 mg, 23%). ^{1}H NMR (300 MHz, $CDCl_3$): δ (ppm) 9.46 (s, 1H, CHO), 7.54 (s, 2H, OH), 7.45 (d, 2H, *J* = 8.9 Hz, ArH), 7.01 (d, 4H, *J* = 7.4 Hz, ArH), 6.85 (d, 4H, *J* = 7.5 Hz, ArH), 6.80 (d, 2H, *J* = 9.0 Hz, ArH), 6.71 (t, 2H, *J* = 7.5 Hz, ArH), 6.63 (t, 2H, *J* = 7.5 Hz, ArH), 4.20 (d, 4H, *J* = 12.9 Hz, $ArCH_2Ar$), 4.07-4.03 (m, 12H, CH_2), 3.80 (t, 4H, *J* = 6.3 Hz, OCH_2), 3.33 (d, 4H, *J* = 13 Hz, $ArCH_2Ar$); ^{13}C NMR (100 MHz, $CDCl_3$) δ (ppm): 190.38, 153.35, 152.94, 151.79, 133.25, 129.22, 128.67, 128.01, 125.69, 125.39, 119.17, 111.09, 76.80, 70.64, 69.38, 52.19, 31.28; MS (ESI): m/z calcd M^+ for $C_{43}H_{43}NO_7$, 685.30; found, 708.45 $(M+Na)^+$.

*Compound **5**:* A solution of compound **4** (505 mg, 1.0 mmol) in ammonia water (10 ml, 28% solution) was stirred for 1 hr. Iodine (279 mg, 1.1 mmol) was added to the above solution and reaction was heated at 40^{o}C for 14 hr. After completion of the reaction, aqueous $Na_2S_2O_3$ (5%) was added to the reaction mixture followed by extraction with methylene chloride. The evaporation of methylene chloride afforded almost pure compound **5** (380 mg, 75%). ^{1}H NMR (300 MHz, $CDCl_3$): δ (ppm) 7.98 (d, 4H, *J* = 1.8 Hz, ArH), 7.56 (t, 2H, *J* = 7.3 Hz, ArH), 7.43 (t, 4H, *J* = 4.0 Hz, ArH), 7.33 (d, 2H, *J* = 9.0 Hz, ArH), 6.63 (d, 2H, *J* = 9.0 Hz, ArH), 4.43 (t, 4H, *J* = 6.3 Hz, OCH_2), 3.72-3.60 (m, 12H, CH_2); ^{13}C NMR (100 MHz, $CDCl_3$) δ (ppm): 166.67, 150.84, 133.73, 133.35, 130.15, 129.82, 128.61, 111.67, 97.79, 69.45, 68.70, 64.05, 51.18. MS (ESI): m/z calcd M^+ for $C_{29}H_{30}N_2O_6$, 502.21; found, 525.35 $(M+Na)^+$.

*Compound **6**:* A solution of compound **5** (502 mg, 1.0 mmol) and aq. NaOH (100 mg, 2.5 mmol, dissolved in 5 ml H_2O) in CH_3OH was refluxed for 14 hr. The solvent was evaporated and the reaction crude was extracted with methylene chloride and water. The methylene chloride layer was dried over anhydrous $MgSO_4$ and evaporated to get pure compound **6** (245 mg, 83%). ^{1}H NMR (300 MHz, $CDCl_3$): δ (ppm) 7.45 (d, 2H, *J* = 8.9 Hz, ArH), 6.69 (d, 2H, *J* = 8.9 Hz, ArH), 3.72-3.64 (m, 12H, CH_2), 3.57 (t, 4H, *J* = 4.7 Hz, OCH_2); ^{13}C NMR (100 MHz, $CDCl_3$) δ (ppm): 151.10, 133.74, 120.79, 111.83, 97.46, 72.83, 68.50, 61.70, and 51.17. MS (ESI): m/z calcd M^+ for $C_{15}H_{22}N_2O_4$, 294.15; found, 317.30 $(M+Na)^+$.

Compound 7: A solution of 4-toluenesulfonyl chloride (476 mg, 2.5 mmol) was added to the mixture of compound **6** (294 mg, 1.0 mmol) and Et_3N (catalytic amount) in dry methylene chloride. The reaction was stirred for 18 hr at room temperature and after completion, the reaction mixture was extracted with water. The organic layer was evaporated and crude was

purified by column (using ethyl acetate: hexane (3: 7)) to afford pure compound **7** (470 mg, 78%). ^{1}H NMR (300 MHz, $CDCl_3$): δ (ppm) 7.76 (d, 4H, *J* = 8.1 Hz, ArH), 7.40 (d, 2H, *J* = 9 Hz, ArH), 7.32 (d, 4H, *J* = 8.5 Hz, ArH), 6.63 (d, 2H, *J* = 9 Hz, ArH), 4.11 (t, 4H, *J* = 3.5 Hz, OCH_2), 3.64-3.55 (m, 12H, OCH_2), 2.44 (s, 6H, CH_3); ^{13}C NMR (100 MHz, $CDCl_3$) δ (ppm): 145.25, 141.45, 133.85, 133.02, 130.15, 129.31, 128.09, 126.26, 113.50, 69.36, 68.92, 68.29, 52.19, 21.88, 21.60; MS (ESI): m/z calcd M^+ for $C_{29}H_{34}N_2O_8S_2$, 602.17; found, 625.35 $(M+Na)^+$.

*Compound **8**:* A mixture of compound **3** (100 mg, 0.14 mmol) and K_2CO_3 (201 mg, 0.14 mmol) in dry CH_3CN was stirred for 30 min at room temperature. Then compound **7** (132 mg, 0.22 mmol) in dry CH_3CN was added to the above mixture and refluxed for 5 days. The solvent was evaporated and the reaction crude was extracted with methylene chloride and water. The organic layer was dried over anhydrous $MgSO_4$, evaporated and purified by column (using ethyl acetate: hexane (1: 1)) to afford pure compound **8** (40 mg, 29%). ^{1}H NMR (300 MHz, $CDCl_3$): δ (ppm) 9.77 (s, 1H, CHO), 7.79 (d, 2H, *J* = 8.8 Hz, ArH), 7.52 (d, 2H, *J* = 8.8 Hz, ArH), 7.10 (d, 8H, *J* = 5.8 Hz, ArH), 3.76 (br, 8H, CH_2), 3.68 (br, 8H, CH_2), 3.57-3.40 (m, 24H, CH_2); ^{13}C NMR (100 MHz, $CDCl_3$) δ (ppm): 190.45, 157.31, 152.69, 150.77, 134.02, 130.71, 126.32, 122.12, 120.91, 111.52, 111.15, 71.71, 70.89, 68.71, 51.47, 51.33, 38.03; MS (ESI): m/z calcd M^+ for $C_{58}H_{61}N_3O_9$, 943.44; found, 966.55 $(M+Na)^+$.

*Compound **9**:* A mixture of compound **8** (100 mg, 0.11 mmol), 2-(2,6-dimethyl-4H-pyran-4-ylidene)malononitrile (20 mg, 0.12 mmol) and piperidine (26 µl, 0.26 mmol) in dry CH_3CN was refluxed for 14 hrs. The color of the solution turned red. The solvent was evaporated, the reaction crude was dissolved in methylene chloride and extracted with water. The organic layer was dried over anhydrous $MgSO_4$, evaporated and purified by column (using ethyl acetate: hexane (2: 3, v/v)) to afford compound **9** (30 mg, 26%). ^{1}H NMR (300 MHz, $CDCl_3$): δ (ppm): 7.49-7.42 (m, 4H, ArH), 7.37 (d, 1H, *J* = 10.34, ArCH), 7.09 (br, 8H, ArH), 6.79-6.60 (m, 10H, ArH), 6.48 (d, 1H, *J* = 10.34, ArCH), 3.73 (br (d), 16H, OCH_2, $ArCH_2Ar$), 3.34 (br, 24H, OCH_2, $ArCH_2Ar$), 2.39 (s, 3H, CH_3); ^{13}C NMR (100 MHz, $CDCl_3$) δ (ppm): 161.94, 160.71, 157.34, 150.84, 149.94, 138.76, 134.02, 133.94, 130.68, 130.23, 122.67, 122.14, 120.82, 115.88, 112.82, 111.97, 106.46, 105.74, 97.86, 71.62, 70.86, 69.02, 68.73, 51.43, 38.07, 29.94, 20.22; MS (ESI): m/z calcd M^+ for $C_{68}H_{67}N_5O_9$, 1097.49; found, 1020.55 $(M+Na)^+$.

NMR and mass spectra:

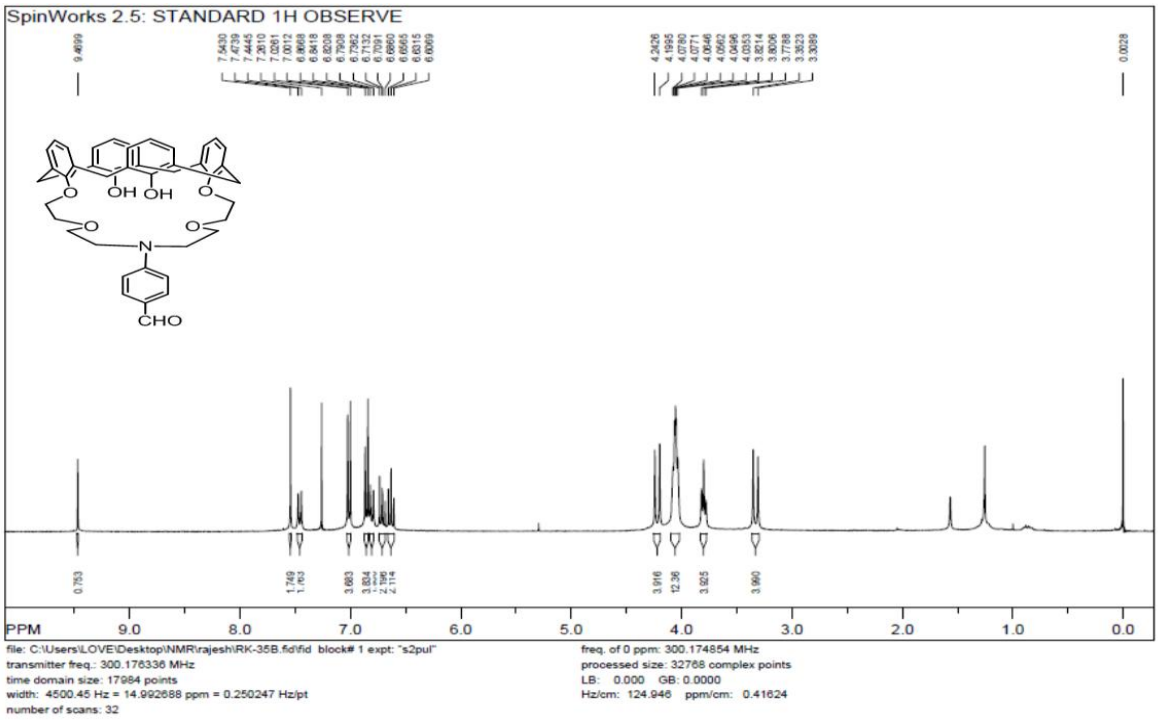

Figure S1. ^{1}H NMR of compound 3 in $CDCl_3$.

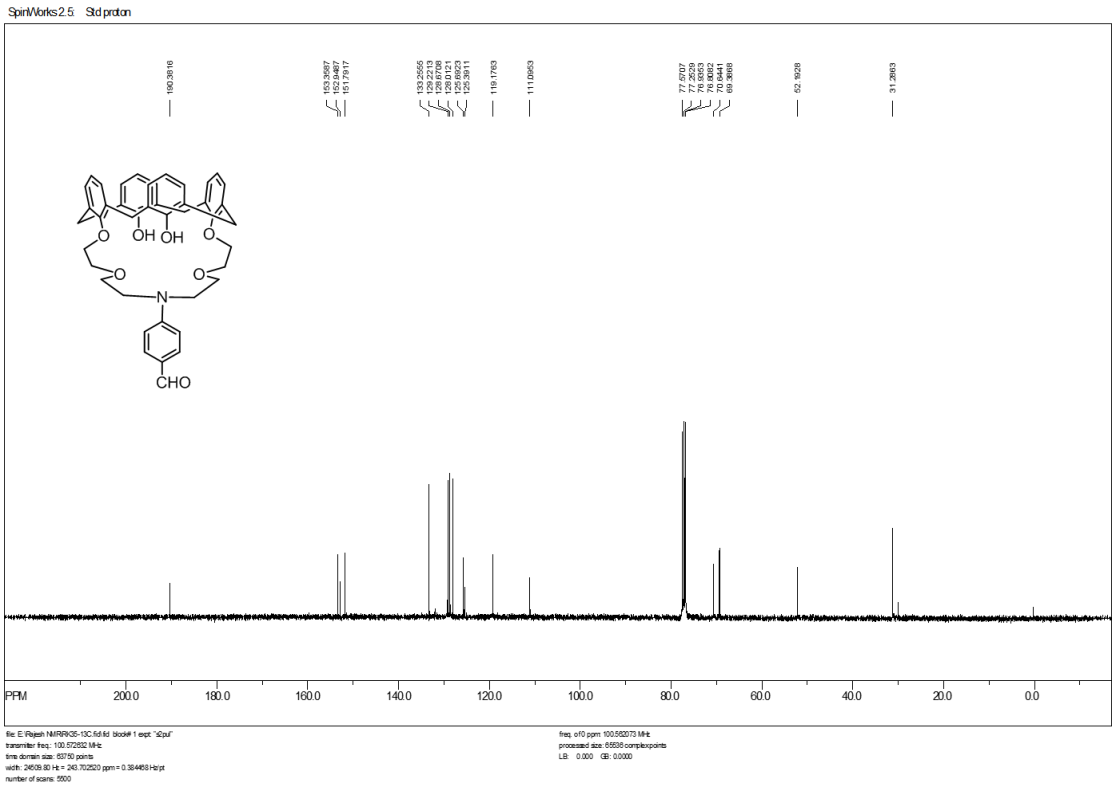

Figure S2. ^{13}C NMR of compound 3 in $CDCl_3$.

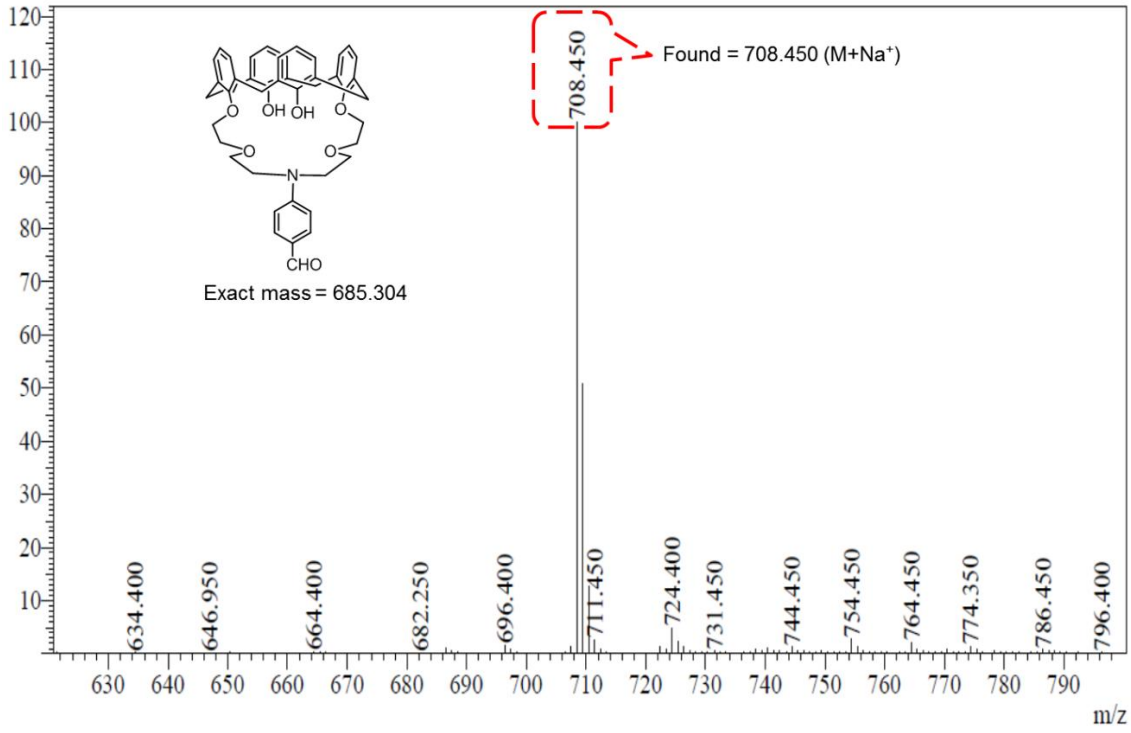

Figure S3. ESI-Mass spectra of compound 3.

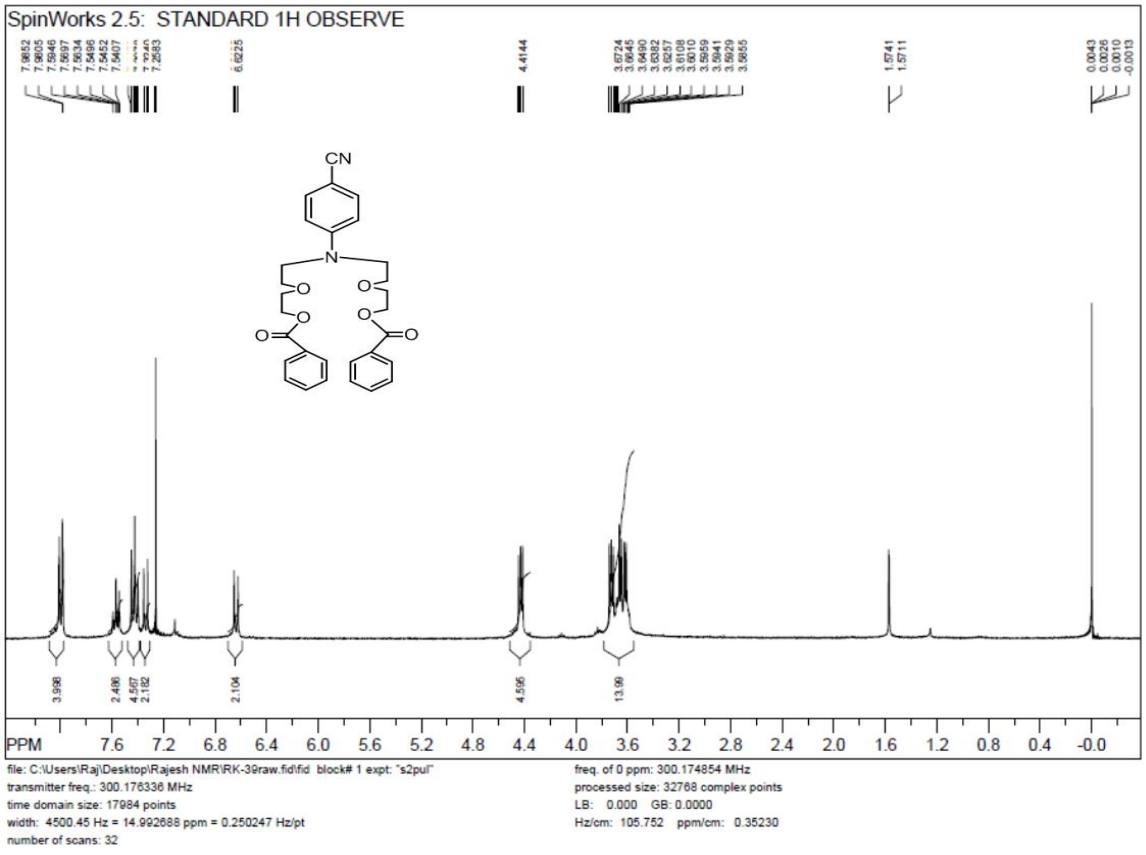

Figure S4. ^{1}HNMR of compound 5 in $CDCl_3$.

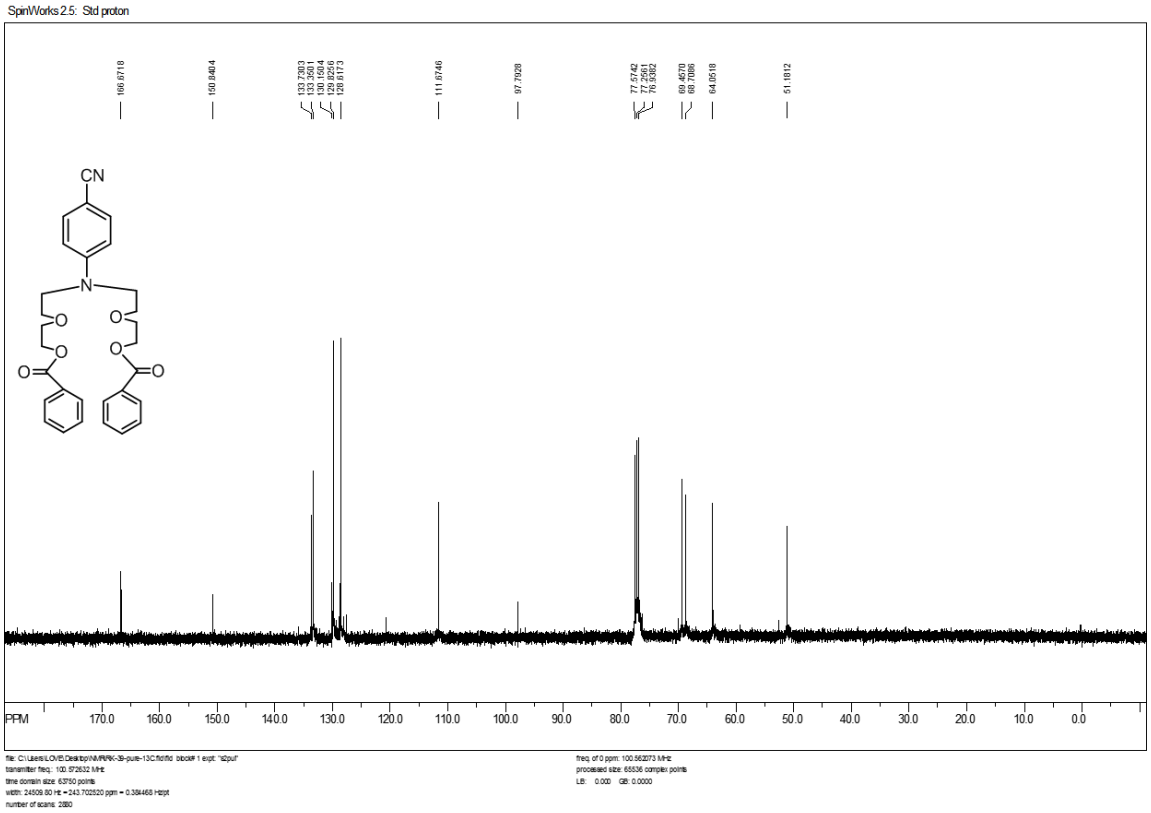

Figure S5. ^{13}C NMR of compound 5 in $CDCl_3$.

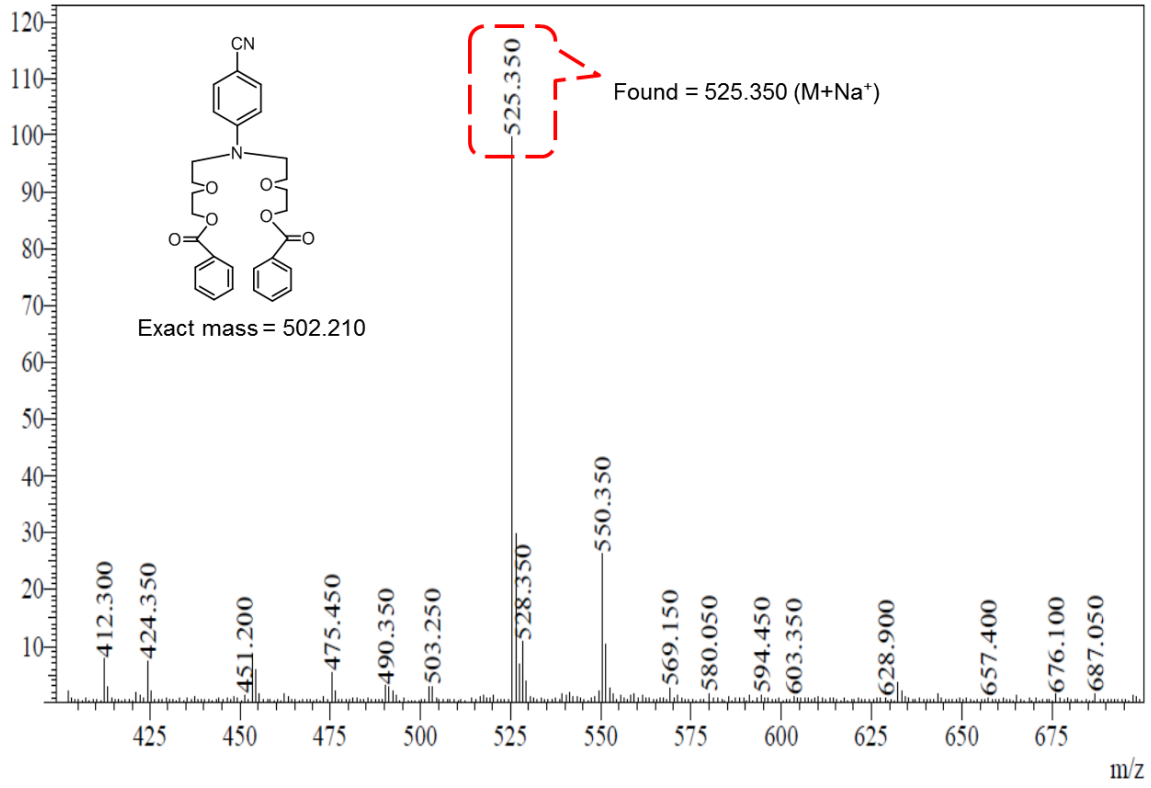

Figure S6. ESI-Mass spectra of compound 5.

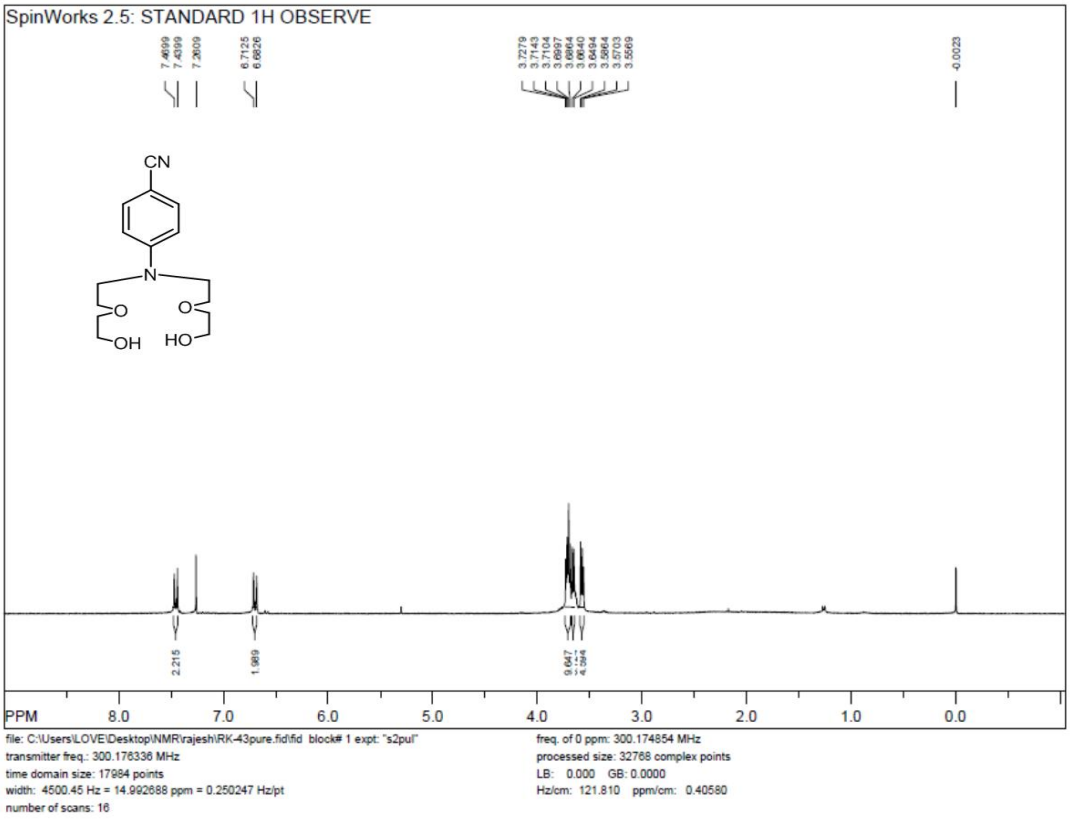

Figure S7. ^{1}H NMR of compound 6 in $CDCl_3$.

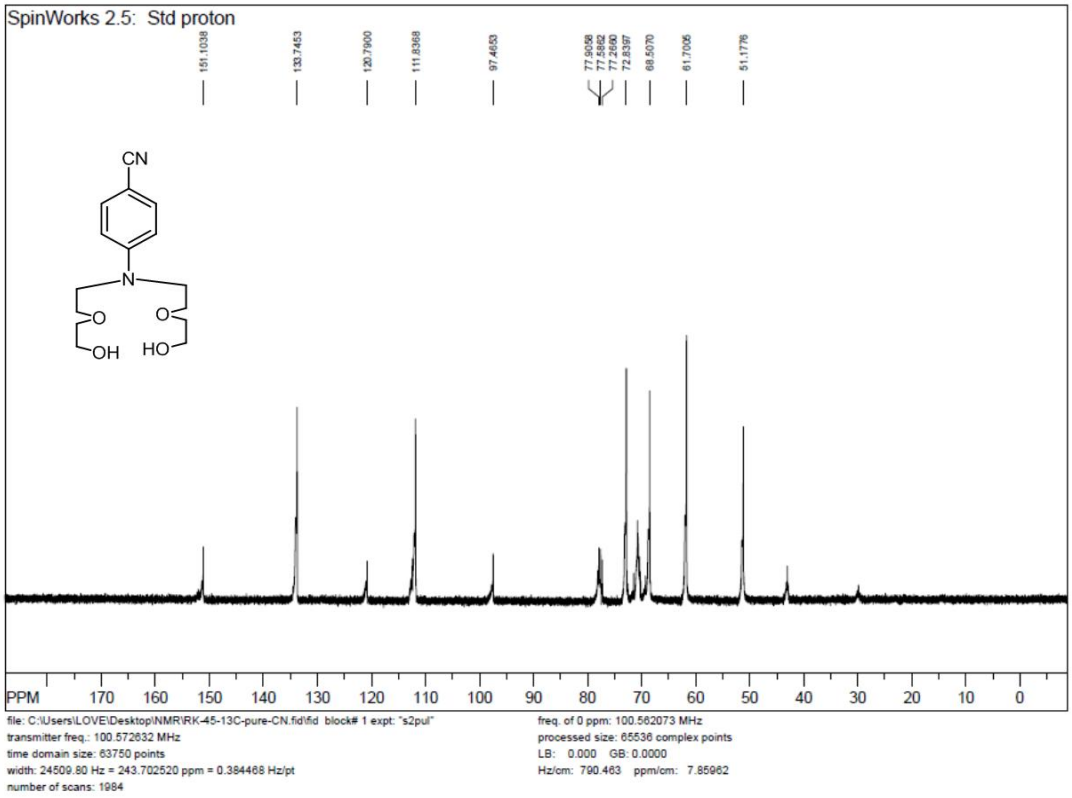

Figure S8. ^{13}C NMR of compound 6 in $CDCl_3$.

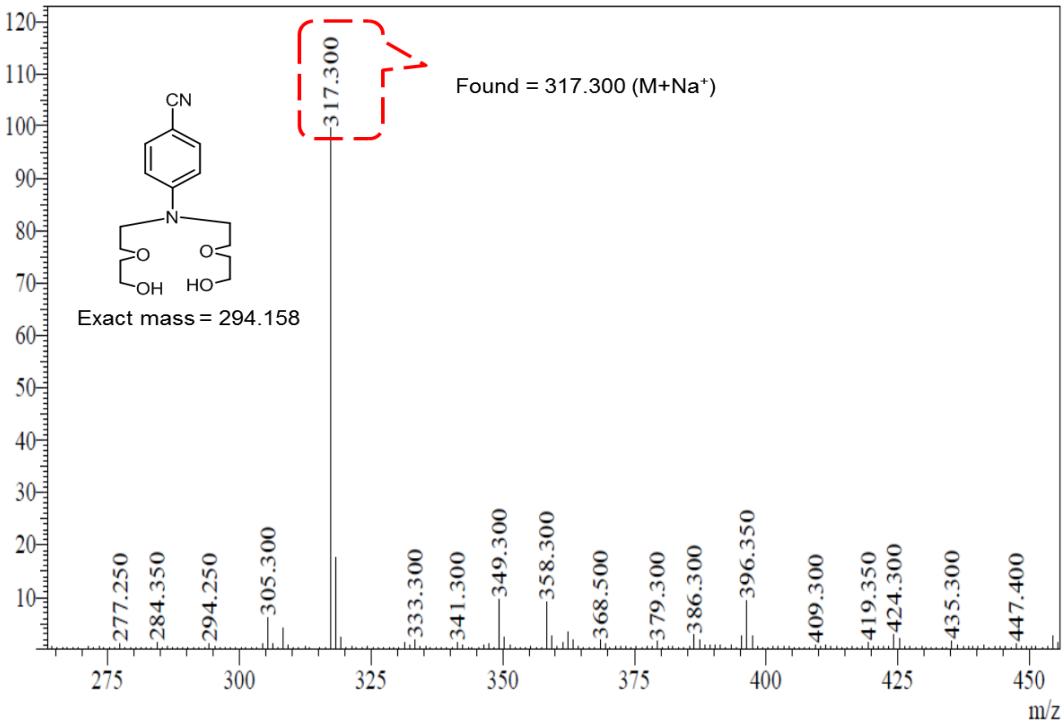

Figure S9. ESI-Mass spectra of compound 6.

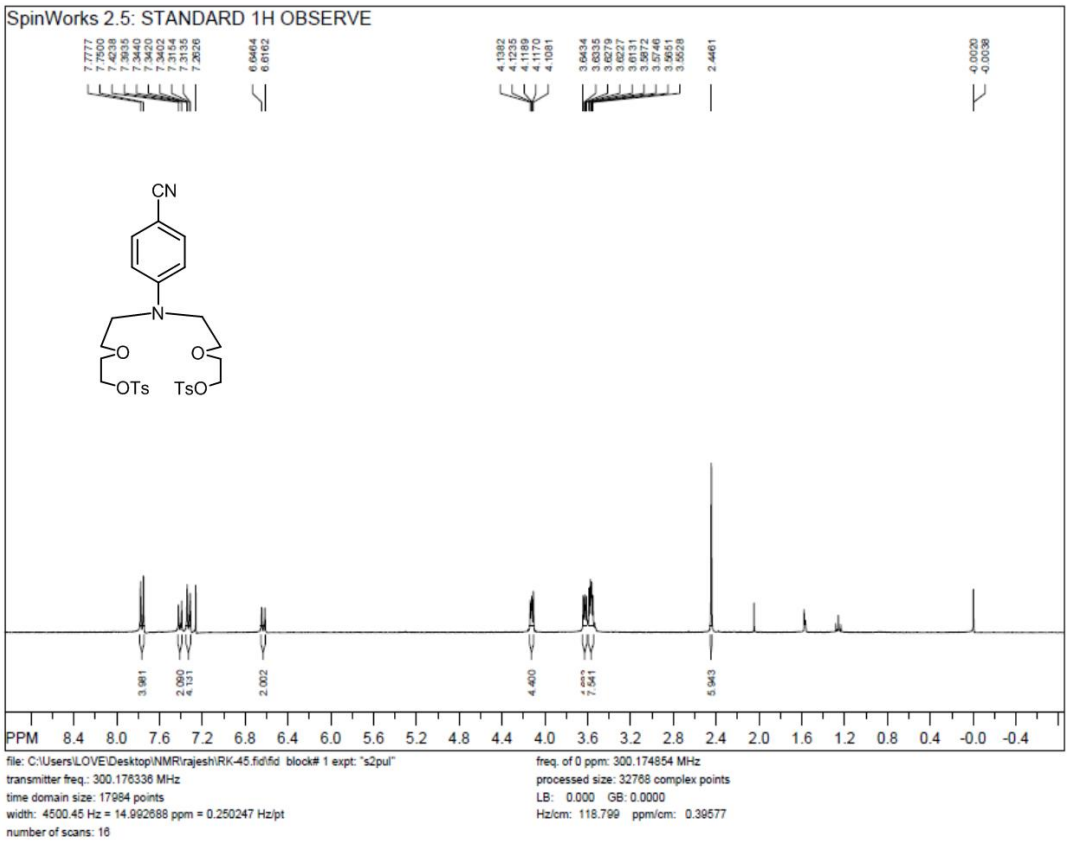

Figure S10. ^{1}H NMR of compound 7 in $CDCl_3$.

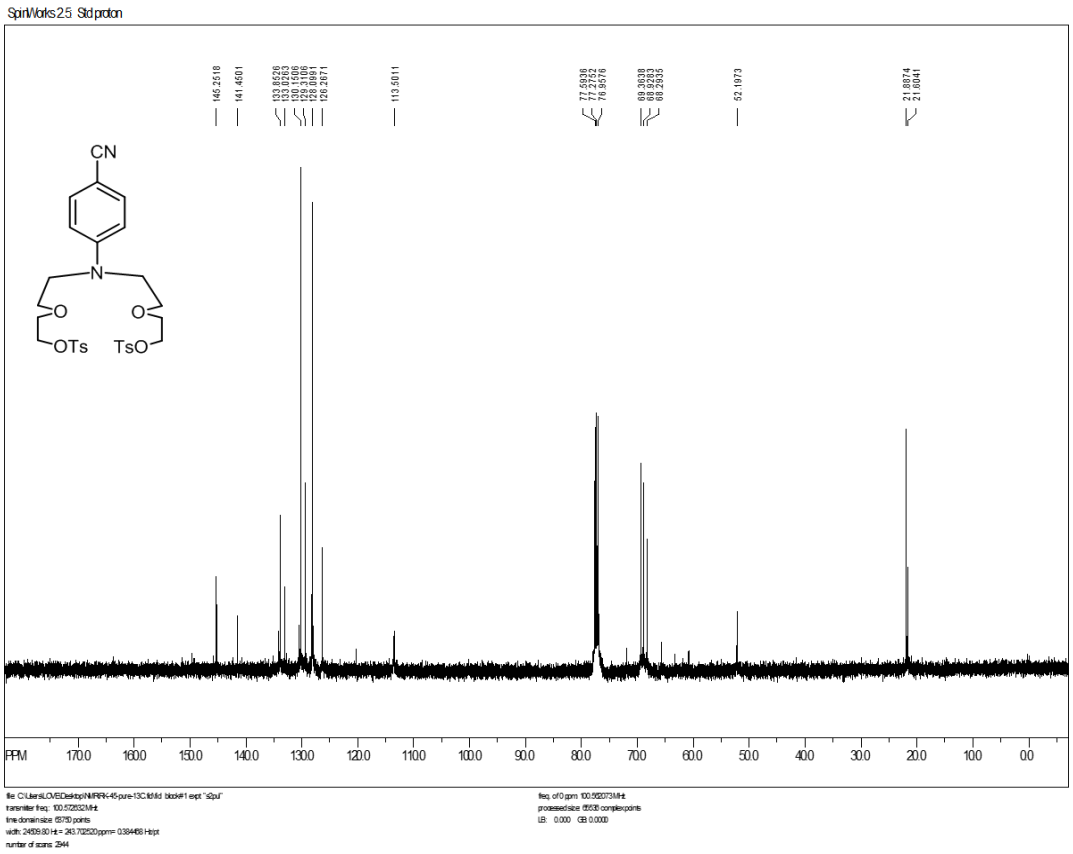

Figure S11. ^{13}C NMR of compound 7 in $CDCl_3$.

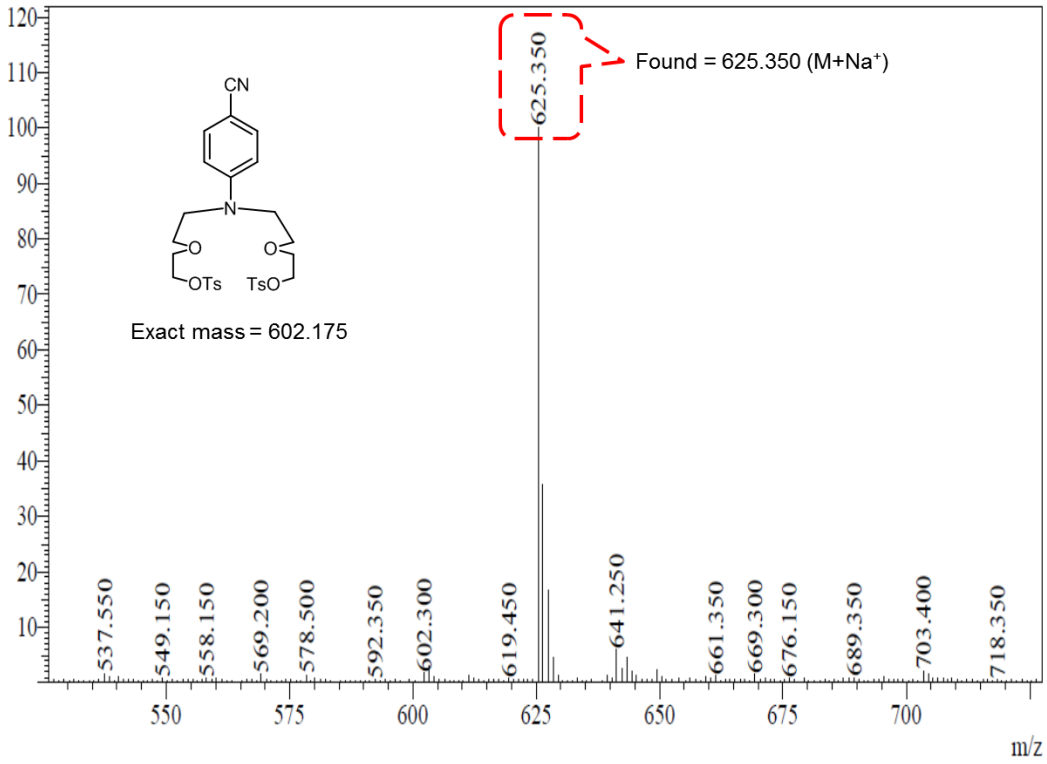

Figure S12. ESI-Mass spectra of compound 7.

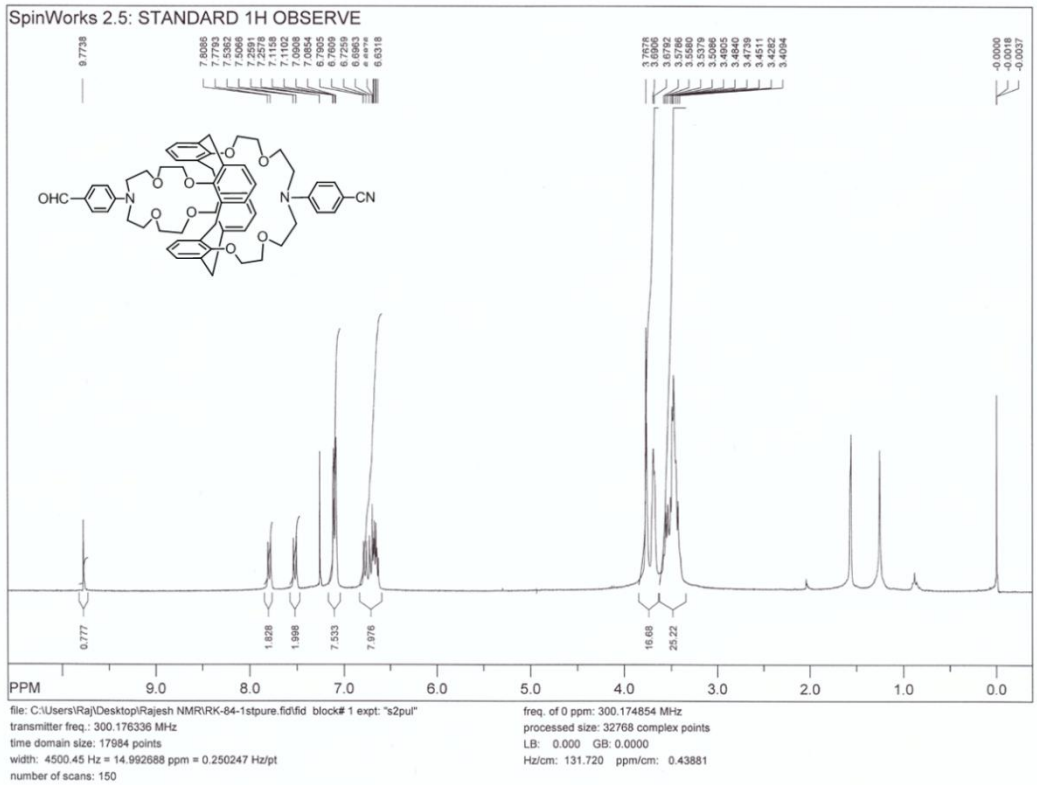

Figure S13. ^{1}H NMR of compound 8 in $CDCl_3$.

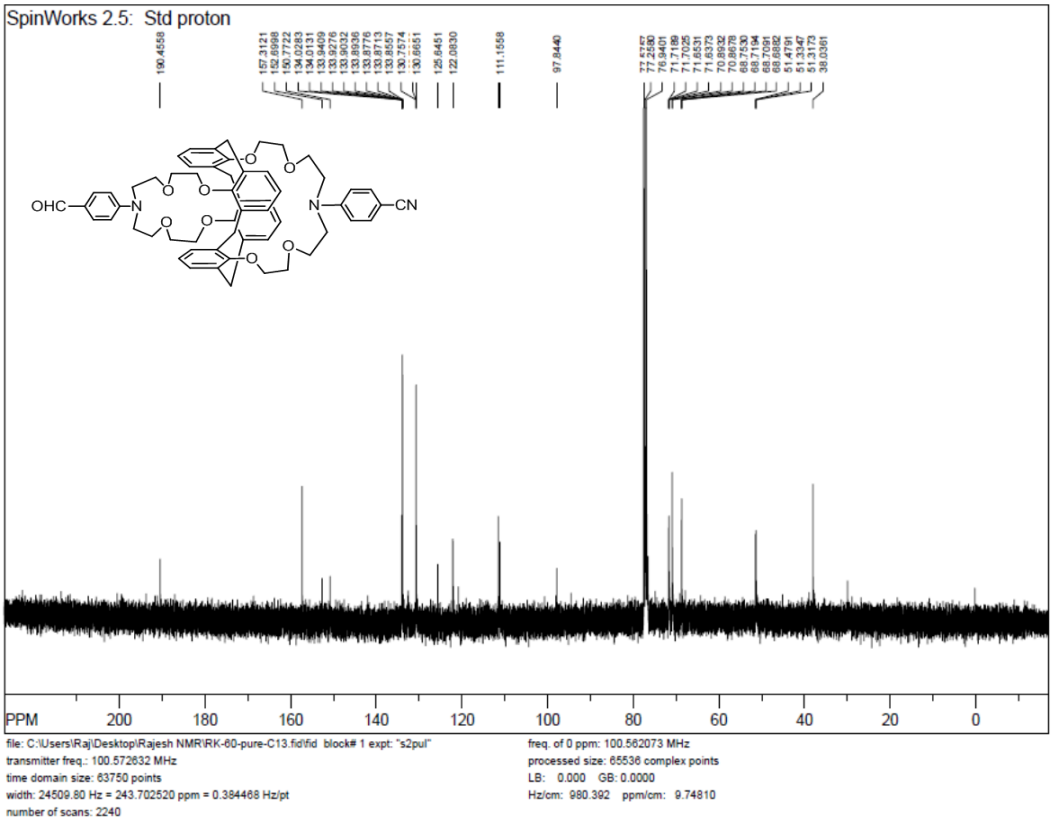

Figure S14. ^{13}C NMR of compound 8 in $CDCl_3$.

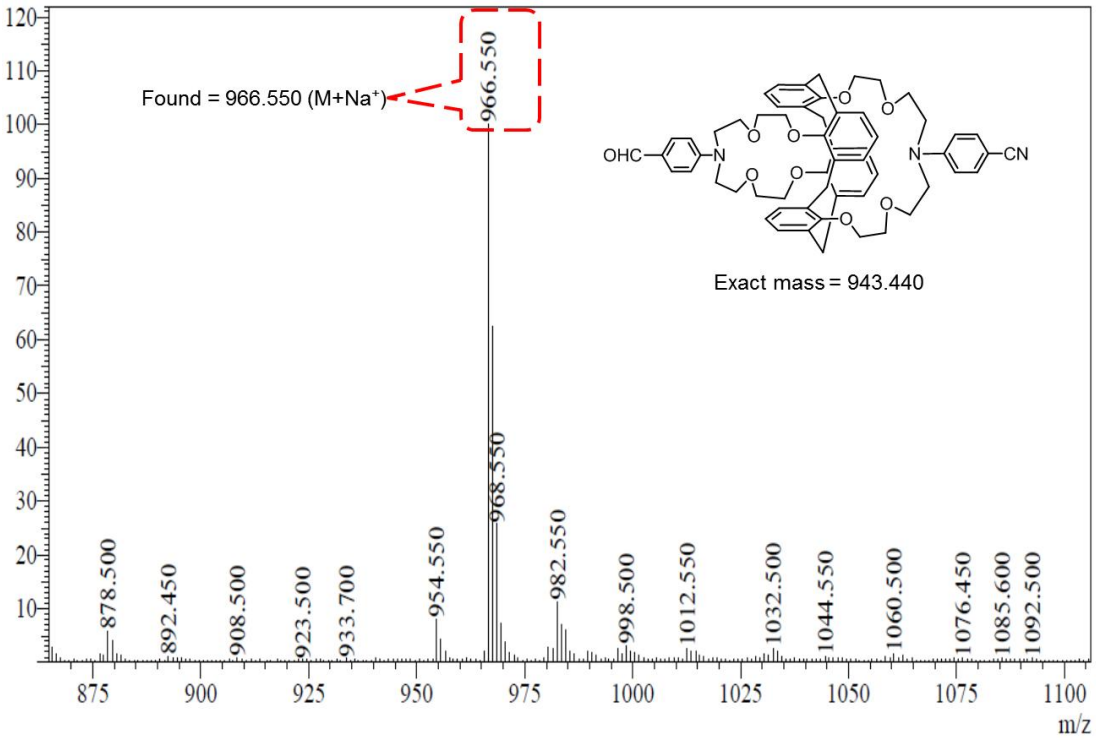

Figure S15. ESI-Mass spectra of compound 8.

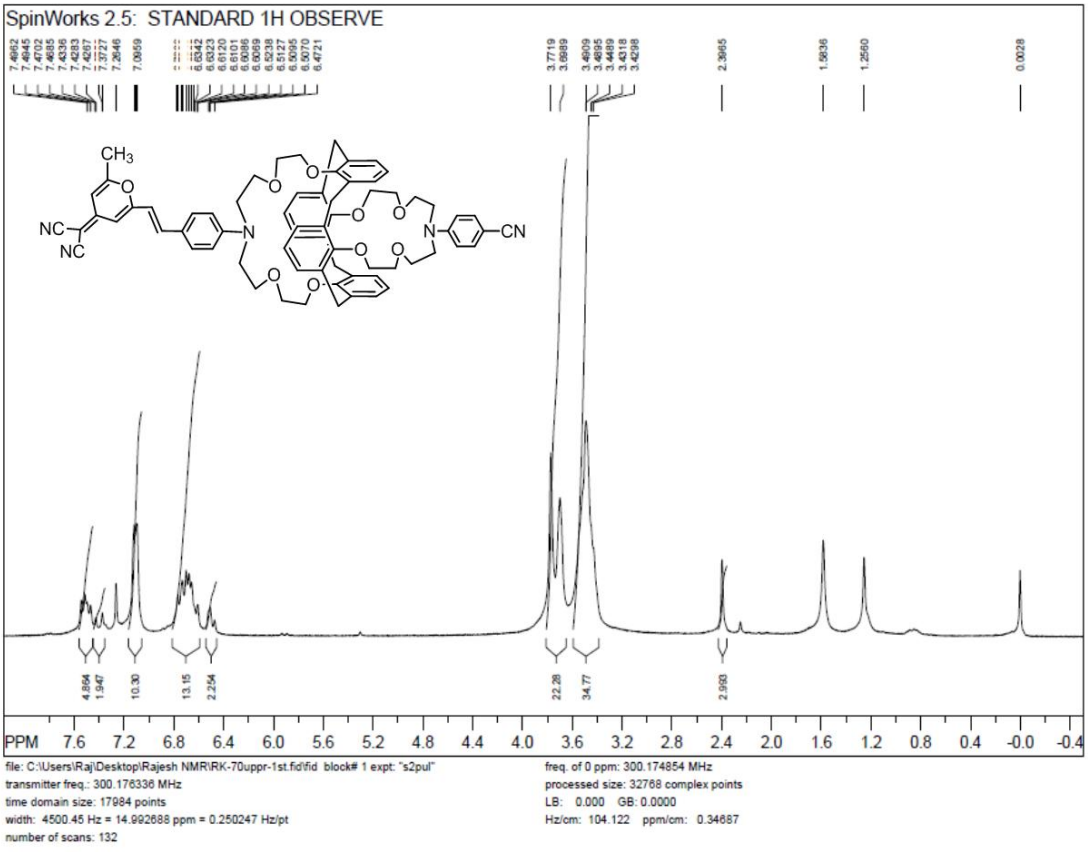

Figure S16. ^{1}H NMR of compound **9** in $CDCl_3$.

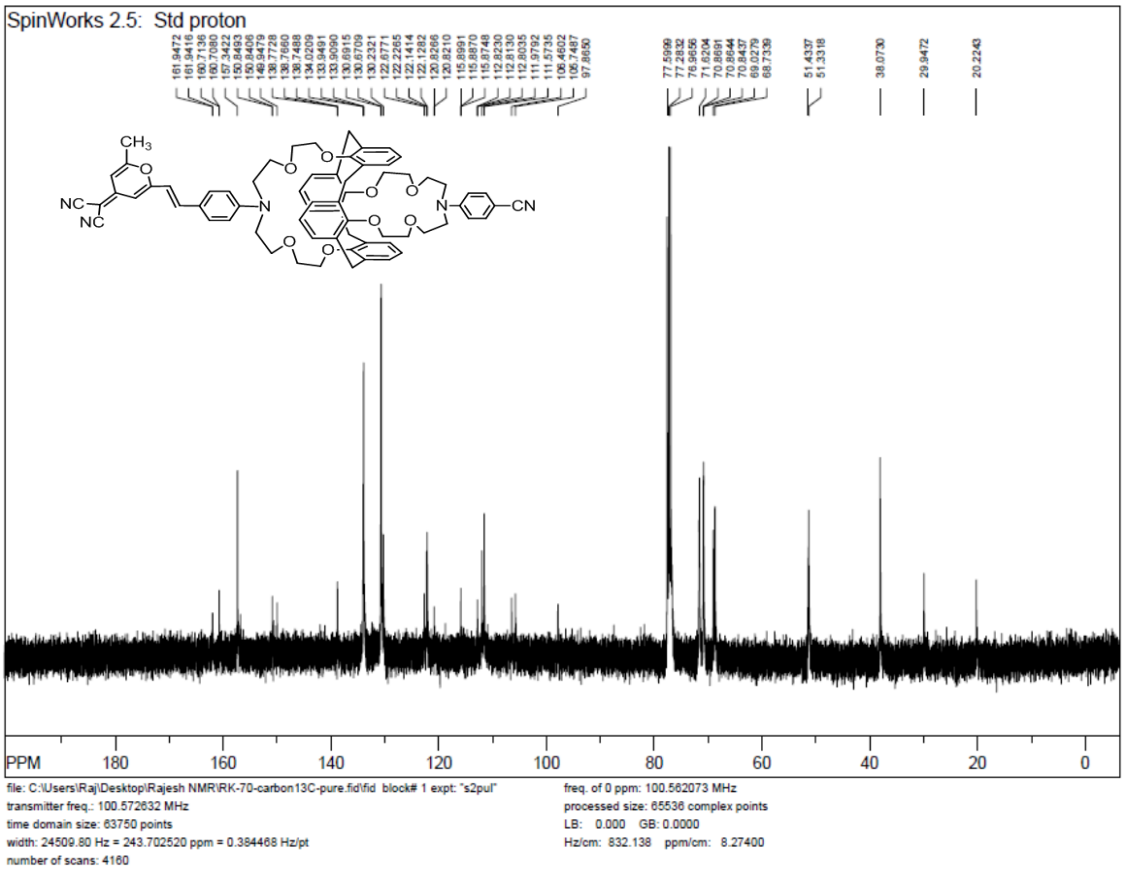

Figure S17. ^{13}C NMR of compound **9** in $CDCl_3$.

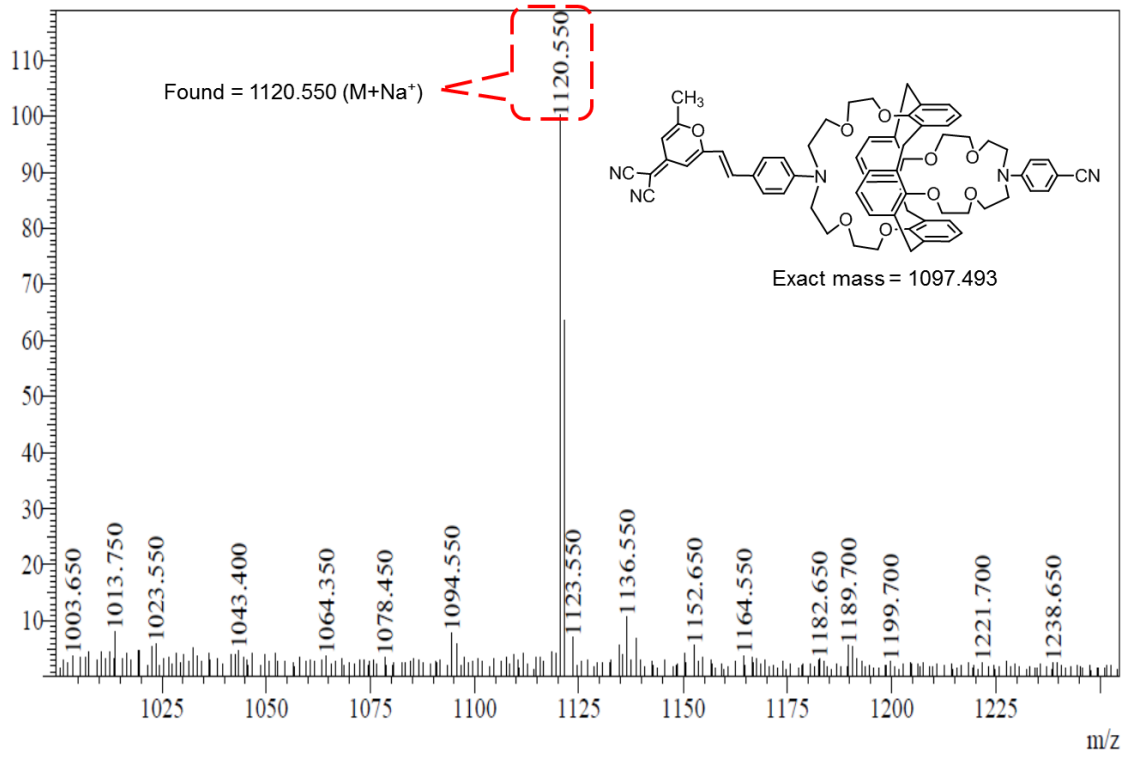

Figure S18. ESI-Mass spectra of compound **9**.

2. NMR study of the complexation of compound 9

The binding behavior of compound **9** towards K^+ ions was investigated by ^1H NMR spectroscopy. Fig. S19 shows ^1H NMR chemical shifts of various protons of compound **9** (5×10^{-3} mol L^{-1} in a 1:1 v/v mixture of CD_2Cl_2 and CD_3CN) upon binding with K^+ ions, at a temperature of 25°C. The addition of 1.0 equivalent of K^+ results in significant shift of various protons of compound **9**. Homologous degenerate protons (l/p, o/s, g/g', h/h', f/j and e/k; see nomenclature in Fig. S19) are particularly interesting to investigate the binding of K^+. These protons display the same shift in the absence of K^+ but are observed to split in the presence of K^+. The NCH_2 protons of both crown rings (l and p) for instance undergo upfield shift upon complexation and appear as a broad doublet with relative shifts of $\Delta\delta$ = -0.24 and -0.17. The OCH_2 protons (o and s) get downfield shifted and also appear as a broad singlets with $\Delta\delta$ = 0.34 and 0.12. Aromatic protons of calix[4]arene (g/i and g'/i') are downfield shifted and split with $\Delta\delta$ = 0.24 and 0.14. Similarly, aromatic protons of phenyl (e/k and f/j) get downfield shifted with $\Delta\delta$ = 0.20 and 0.05 (for e/k) and 0.13 (for f/j). These observations prove that complexation occurs as expected, although they do allow to determine the exact localization of the bound cation: *i.e.* on the DCM side or on the DMABN side, or both.

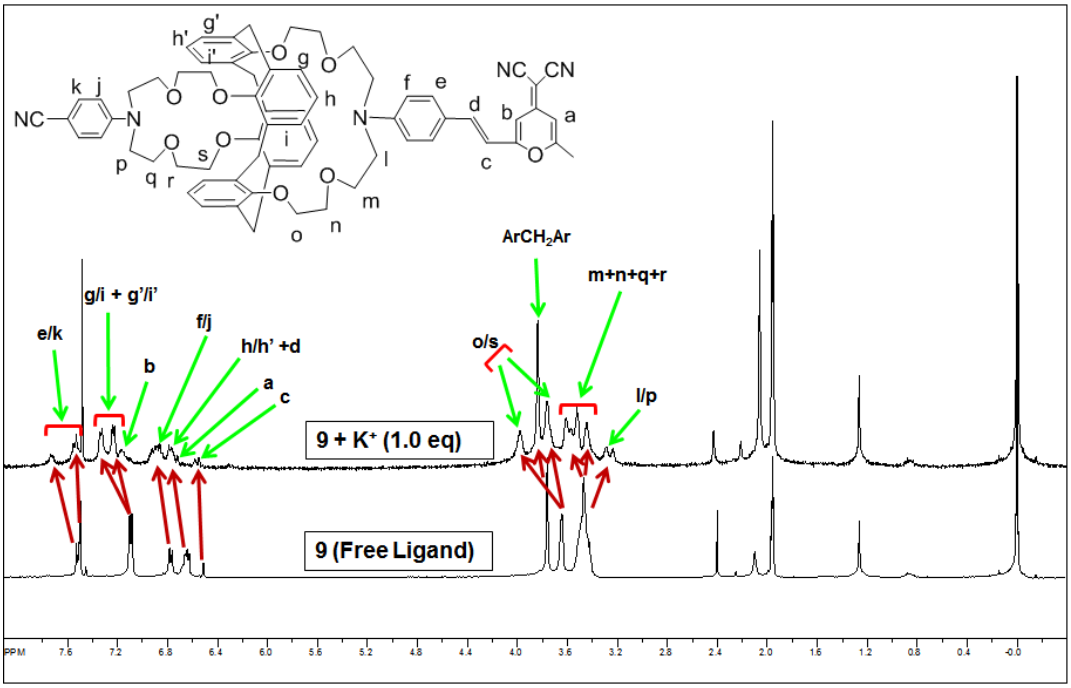

Figure S19. ^1H NMR spectra (400 MHz) of compound **9** after addition of 1.0 equiv of KSCN in $CDCl_3$/ CD_3CN (1/1, v/v) at 25°C.

The precise localization of the K^+ ion in the 1:1 complex, together with the determination of the relevant association constants, was achieved by UV/Vis absorption spectroscopy, as described in the following section (§3).

3. Complexation model

3.1. Theory

The UV/Vis absorption spectra of compound **9** upon titration by KSCN (main text, Fig. 1A) were recorded on a Varian Cary 300 spectrophotometer. The complexation constants and the spectra of the different species were determined by global analysis of the full set of spectra by using a homemade Mathematica program.

In brief, the spectra were first fitted using a two-site complexation model presented below. A weighted average absorption coefficient of the two 1:1 complexes (ML_{DCM} and ML_{DMABN}), noted ε_{ML} (Fig. 1B, blue line), was then obtained. The relative concentrations of ML_{DCM} and ML_{DMABN} were finally deduced by fitting ε_{ML} with a sum of spectra chosen to represent ML_{DCM} and ML_{DMABN} in the region of DCM absorption.

Definitions:

We use a complexation model taking into account the two different sites of complexation, *i.e.* the formation of the ML_{DCM} and ML_{DMABN} complexes with two different equilibrium constants:

$M + L \rightleftharpoons ML_{DCM}$, with constant K_1

$M + L \rightleftharpoons ML_{DMABN}$, with constant K_1'

We assume that the two complexes are in equilibrium:

$ML_{DCM} \rightleftharpoons ML_{DMABN}$, with constant K_e (called equilibrium constant of exchange).

For the complexation of a second K^+ ion we have:

$M + ML_{DCM} \rightleftharpoons M_2L$, with constant K_2.

$M + ML_{DMABN} \rightleftharpoons M_2L$, with constant K_2'.

Equilibria:

The above system is fully determined by only three of these equilibria. We chose: K_1, K_e and K_2. Elementary calculations show that:

$K_1' = K_1\, K_e$ and $K_2' = K_2 / K_e$

Conservation relations:

The conservation of the total concentrations of ligand $[L]_0$ and metal $[M]_0$ can be written as follows:

$$[L]_0 = [L] + [ML_{DCM}] + [ML_{DMABN}] + [M_2L] \quad (4)$$

$$[M]_0 = [M] + [ML_{DCM}] + [ML_{DMABN}] + 2[M_2L] \quad (5)$$

Change of variables:

To simplify the system we defined three new variables:

$[ML] = [ML_{DCM}] + [ML_{DMABN}] = [ML_{DCM}](1 + K_e)$ (total concentration of 1:1 complexes)

$K_a = K_1 + K_1' = K_1(1 + K_e)$

$1/K_b = 1/K_2 + 1/K_2'$ hence $K_b = K_2/(1 + K_e)$

It is straightforward to show that:

$$K_a = \frac{[ML]}{[M][L]} \text{ and } K_b = \frac{[M_2L]}{[M][ML]} \quad (7)$$

Equations (4) and (5) can be rewritten with the new variables:

$$[L]_0 = [L] + [ML] + [M_2L] \quad (8)$$

$$[M]_0 = [M] + [ML] + 2[M_2L] \quad (9)$$

Beer-Lambert's law:

The absorption (A) of the sample in the presence of the four relevant species is described by Beer-Lambert's law:

$$A/\ell = \varepsilon_L[L] + \varepsilon_{MLdcm}[ML_{DCM}] + \varepsilon_{MLdmabn}[ML_{DMABN}] + \varepsilon_{M2L}[M_2L] \quad (10)$$

(where ℓ is the length of the sample cuvette).

Using the new variables, one gets:

$$A/\ell = \varepsilon_L[L] + \varepsilon_{ML}[ML] + \varepsilon_{M2L}[M_2L] \quad (11)$$

where:

$$\varepsilon_{ML} = (\varepsilon_{MLdcm} + K_e\,\varepsilon_{MLdmabn})/(1 + K_e) \quad (12)$$

3.2. Analysis of the titration data

The spectra of Fig. 1A (main text) were globally fitted to equation (11), using an exact solution of equations (7), (8) and (9). We obtained the spectra of the free ligand (ε_L), of the total 1:1 complex (ε_{ML}) and of the 2:1 complex (ε_{M2L}) (cf. Fig. 1B, main text). The optimal values of K_a and K_b were found to be, in decimal log form:

$\log K_a = 3.56 \pm 0.01$ and $\log K_b = 1.0 \pm 0.4$.

We next analyzed the ε_{ML} spectrum using equation (12) in order to obtain the value of K_e. In the region of the DCM chromophore absorption (350-600 nm), where DMABN does not

contribute, we made the assumption that ε_{MLdcm} can be approximated by the absorption coefficient of species ML of Calix-DCM2 ($\varepsilon_{ML}^{Calix-DCM2}$).[1] Similarly, we assumed that $\varepsilon_{MLdmabn}$, which corresponds to an uncomplexed DCM species, can represented by the absorption coefficients of species L of Calix-DCM2 ($\varepsilon_{L}^{Calix-DCM2}$).

A first fit of ε_{ML} spectrum using equation (12) and the above assumptions yielded $K_e = 0.051 \pm 0.006$ but with a relatively poor quality (large residues; not shown). To improve the fit we allowed $\varepsilon_{ML}^{Calix-DCM2}$ to be multiplied by an adjustable coefficient (parameter *a*). A good fit, shown in Fig. S20, was obtained with $a = 0.93$; it yielded $K_e = 0.053 \pm 0.002$, which is very close to the previous determination and hence gives high confidence in a value of the order of 5%. Parameter *a* suggests that ε_{MLdcm} in compound **9** has the same shape as $\varepsilon_{ML}^{Calix-DCM2}$ but a slightly different amplitude (possibly due to a slightly different interaction of the cation with the crown on the DCM side).

The small value of K_e shows that the equilibrium is strongly displaced towards ML_{DCM}. The binding of K^+ on the DMABN side is thus much less favorable than on the DCM side.

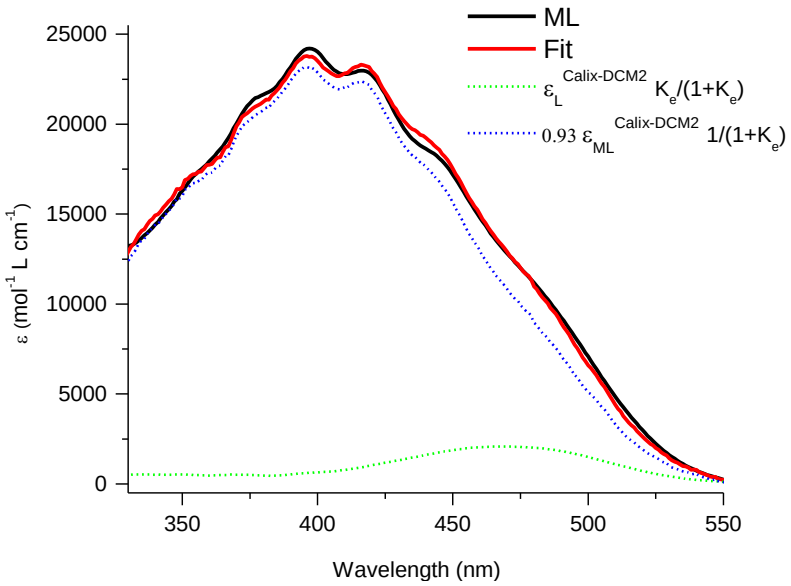

Figure S20. Fit of ML using equation (12) and a set of assumptions to represent ε_{MLdcm} and $\varepsilon_{MLdmabn}$ in the spectral region of DCM absorption (see text). The ML spectrum is shown in black and the fit in red. The contributions proportional to $\varepsilon_{L}^{Calix-DCM2}$ and $\varepsilon_{ML}^{Calix-DCM2}$ and are shown in green and blue dotted lines, respectively.

Fig. S21 shows the expected molar fractions of the four species (L, ML_{DCM}, ML_{DMABN} and M_2L) for the titration shown in Fig. 1A (main text).

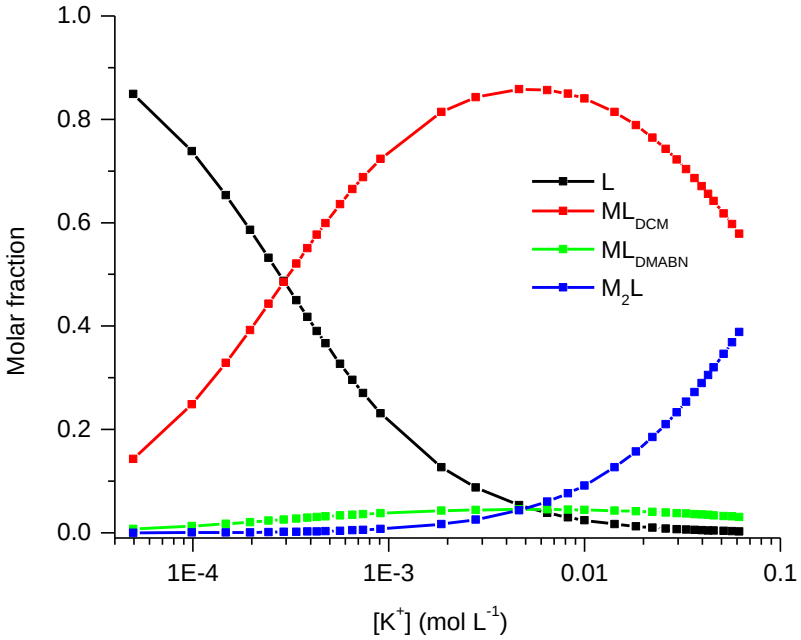

Figure S21. Molar fractions of L, ML_{DCM}, ML_{DMABN} and M_2L.

3.3. Comparison with Calix-DCM2

It is interesting to compare the equilibrium constants obtained for compound **9** and Calix-DCM2. For compound **9** we have seen that:

$\log K_a = 3.56$ and $K_e = 0.05$.

The constant corresponding to the complexation of one K^+ ion on the DCM side of the molecule is thus: $\log K_1 = \log K_a - \log(1 + K_e) = 3.54$.

For Calix-DCM2 the two sites are equivalent, so $K_e = 1$. In our previous paper we have shown that $\log K_a = 3.81$,[1] which yields to $\log K_1 = 3.51$ for the binding of K^+ on one side only of the molecule. This shows that the binding of one K^+ ion on the DCM side is very similar on both molecules.

4. Transient absorption spectroscopy

4.1. Setup

Samples for the transient absorption measurements were prepared as follows. Free compound **9** (L) was diluted in neat acetonitrile, at a concentration of 86×10^{-6} mol L^{-1}. The complex solution (ML90) was prepared by diluting compound **9** in KSCN-containing acetonitrile. The total concentration of compound **9** was 164×10^{-6} mol L^{-1}, and that of K^+ was 5.3×10^{-3} mol L^{-1}. At these concentrations the results of the spectrophotometric titration predict: [L] = 8×10^{-6}

mol L^{-1} (4.8% of total compound **9**), [ML] = 148×10^{-6} mol L^{-1} (90.4% of total compound **9**, with 95% of K^+ complexed on the DCM side) and [M_2L] = 8×10^{-6} mol L^{-1} (4.8% of total compound **9**). These concentrations were confirmed by fitting the absorption spectrum with the absorption spectra of the different species.

Femtosecond transient absorption spectra were recorded by the pump–continuum-probe technique. A pump pulse at 387.5 nm was used to excite the sample and the photoinduced dynamics was probed by a polychromatic probe pulse allowing to record absorption spectra from 360 to 750 nm. The kinetics were obtained by scanning the pump-probe delay, with a motorized optical delay line. The maximum delay available with our setup is 1.5 ns. The temporal resolution of the experiment is determined by the temporal overlap of the pump and the probe beam: in this experiment it was of the order of 120 fs.

The source was an amplified Ti:Sapphire laser system (Tsunami and Spitfire, Spectra Physics), delivering 50 fs pulses at 810 nm and 1 kHz. Part of this beam was used to generate the 387.5 nm pump beam by frequency doubling in a BBO crystal. The excitation energy (0.026 µJ) was chosen in the linear regime so that multiphotonic excitation can be excluded. The polychromatic probe beam was generated by focusing a few mJ pulse of the 810-nm beam on a moving CaF_2 plate. The continuum was split into a sample and a reference beam. The sample probe beam was focused by a 90° off-axis parabolic mirror onto the sample cell and crossed the pump beam at an angle of ~5°. The 1 mm thick fused-silica cuvette containing the sample was translated in 2D in order to make sure that consecutive laser pulses do not irradiate the same sample volume. The linear polarizations of the pump and probe beams were set at the magic angle. The transmitted reference and sample probe beams were focused onto the entrance slit of an imaging spectrograph (Acton SP300i, 150 grooves mm^{-1}). The spectra were recorded on a CCD detector (Pixis-100B, 100×1340 pixels, Roper Scientific).

The measurements provide differential absorbance spectra defined as the difference between the absorbance of the excited sample and that of the unexcited sample. These spectra were corrected from the chirp of the probe beam—*i.e.* difference of arrival time of the different wavelengths, arising from group velocity dispersion in the material media the probe beam passes through before reaching the sample. The probe wavelengths affected by scattering of the pump beam by the sample cuvette were removed prior to data analysis and masked in the figures.

Let us also note that during pump-probe overlap (a couple hundred fs) a strong artifact overlaps the pure molecular signal. It is called cross-phase modulation (XPM) and is due to the modulation of the refraction index of the sample by the pump beam.

Let us finally recall that the transient absorption signal is a sum of three "pure" contributions: Excited-state absorption (ESA: the absorption of excited, or transient, state to higher lying excited states, yielding positive bands), Stimulated emission (SE: the emission transitions from excited states to lower lying states (generally ground state); gives rise to negative bands in the spectra (usually found in the region of fluorescence) and Ground-state bleaching (GSB: negative band in the region of the steady-state absorption, due to the fact that a fraction of the molecules in the ground state are missing after excitation). For short we will name ESA, SE or GSB bands, (respectively positive, negative or negative) net bands dominated by pure ESA, SE or GSB signals, which does not exclude the presence of minority contributions of different nature.

4.2. Free ligand

The transient absorption spectra of the free ligand (L) of compound **9** in acetonitrile, recorded after sub-100-fs excitation at 387.5 nm, are shown in Fig. S22.

Between -0.3 and 0.2 ps (Fig. S22A) the transient absorption signal rises as the overlap of the pump and probe pulses (0.12 ps HWHM) builds up. A positive excited-state absorption (ESA) band grows at 475 nm together with a negative stimulated emission (SE) band around 612 nm. During this step, a sharp negative peak is observed around 443 nm, only observed while the pump and probe pulses temporally overlap. It is due to stimulated Raman scattering from the solvent. Other sharp features are also temporarily seen in the blue part of the spectrum. They arise from the so-called cross-phase modulation artifact (XPM). It is interesting to note that a new positive ESA band starts to grow around 530 nm between 0.1 and 0.2 ps.

Between 0.2 and 2 ps (Fig. S22B) the spectra further evolve. The ESA band at 530 nm continues to grow together with an ESA band at 410 nm. A dip appears at 500 nm. It likely corresponds to the overlap of a broad positive ESA contribution (spanning from 410 to 530 nm) and the negative contribution of ground-state bleaching (GSB). The SE band continues to grow and it shifts to the red (from 610 to 625 nm). A temporary quasi-isosbestic point is observed at 510 nm, suggesting that the initially excited state gives rise to a new excited state, the stimulated emission of which is observed around 625 nm. It may in fact be noted that

spectrally drifting, "loose" isosbestic points are seen around 463 and 594 nm. They might actually result from the crossing of spectrally-shifting bands (see discussion below).

Between 2 and 100 ps (Fig. S22C) the spectra do not undergo any major change, except for a small decrease observed in all bands.

Between 100 and 1400 ps (Fig. S22D) all bands substantially decrease. A red shift is observed for the SE band (from 630 to 637 nm) and a quasi-isosbestic point is observed at 565 nm.

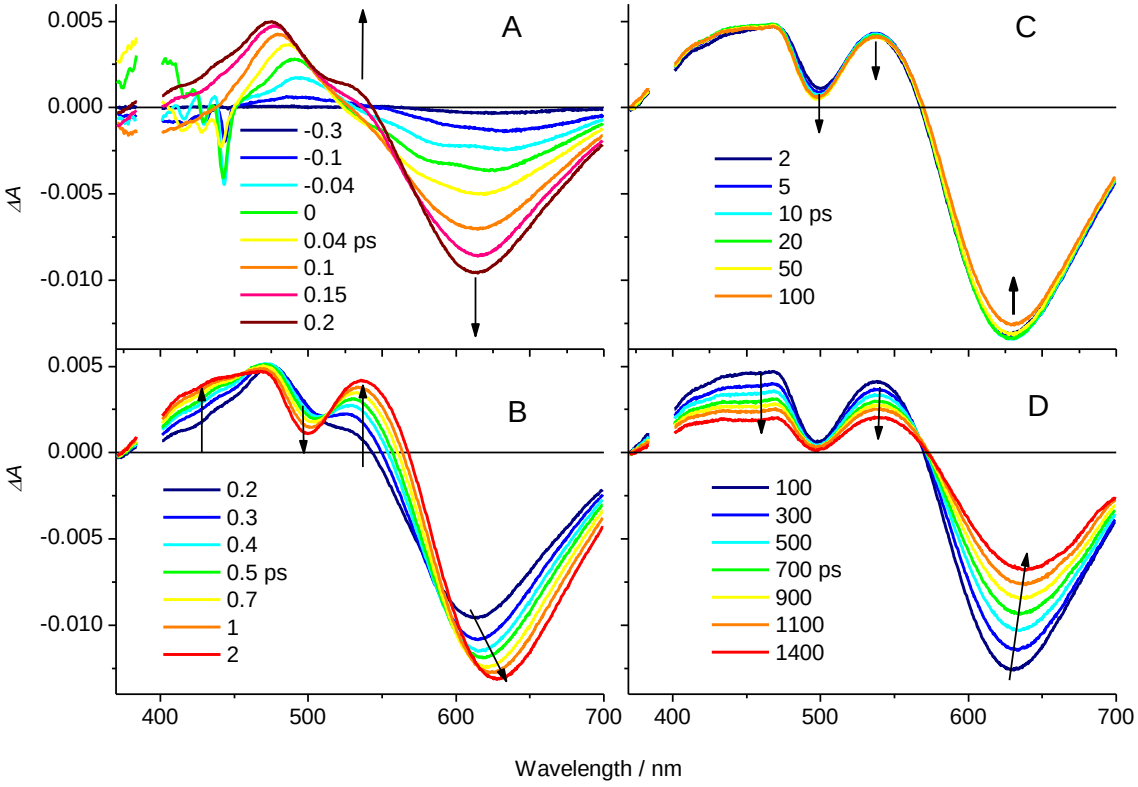

Figure S22. Transient absorption spectra of free compound **9** in acetonitrile, after excitation at 387.5 nm, for pump delays ranging from -0.3 to 0.2 ps (A); from 0.2 to 2 ps (B); from 2 to 100 ps (C) and from 100 to 1400 ps (D).

4.3. ML90 sample

As detailed in §4.1 the sample used to study the 1:1 complex contained 86% of ML_{DCM} complex, in which K^+ is bound to the DCM side of the molecule. This sample will be referred to as ML90 because it can be calculated that ~90% of the initially excited molecules are ML_{DCM} complexes (by taking into account the absorption coefficient of the different species (Fig. 1B, main text) at the excitation wavelength (387.5 nm)). In the following, it will be assumed for simplicity that the transient absorption spectra recorded for the ML90 sample, given in Fig. S23, are due to the excitation of ML_{DCM} only.

As a general guideline to the comparison of the ML90 and L spectra, it should be kept in mind that the bleaching contribution in the two cases are distinct: it is about 60 nm blue shifted for ML_{DCM} as compared to L.

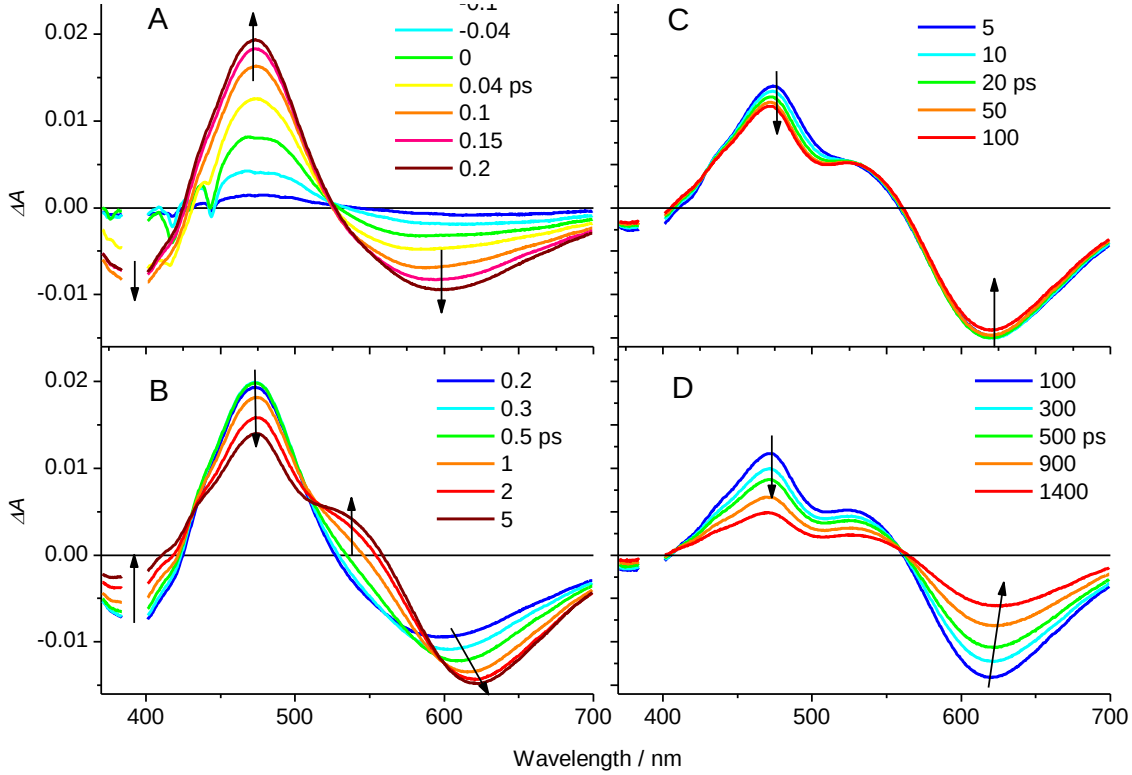

Figure S23. Transient absorption spectra of the ML90 sample of compound **9** in acetonitrile, after excitation at 387.5 nm, for pump delays ranging from -0.3 to 0.2 ps (A) and from 0.2 to 10 ps (B). for pump delays ranging from 10 to 100 ps (C) and from 100 to 1400 ps (D).

Between -0.3 and 0.2 ps (Fig. S23A) one observes the growth of the signal, accompanied with sharp peaks and wiggles assigned to stimulated Raman scattering of the solvent and XPM. An ESA band grows at 470 nm and an SE band at 600 nm. A GSB band is observed between 360 and 420 nm, dominated by the bleaching of ML_{DCM}.

More changes are observed between 0.2 and 5 ps (Fig. S23B). An ESA band appears at 530 nm. The GSB band concomitantly decreases. Note that this does not necessarily mean that ground-state recovery occurs; the growth of an ESA band in the same region could produce the same effect. The SE band continues to grow and substantially shifts to the red, from 600 to 620 nm. Quasi-isosbestic points are observed at 431 nm and around 510 nm (the second one is not so well defined and actually drifts towards the red).

Between 5 and 100 ps the spectra do not undergo major changes. A moderate decrease of the main bands is observed (Fig. S23C). The SE band very slightly shifts to the blue (by ~2 nm). Between 100 and 1400 ps all bands decrease (Fig. S23D). A small red shift is observed for the SE emission band: from 620 to 625 nm.

5. Global analysis of the transient absorption spectra

5.1. Method

Global, multiexponential kinetic analysis,[2] where the same time constants are shared at all wavelengths, was performed as follows. Singular value decomposition[3] (SVD) was first done on the matrix containing the two-way (wavelength and time) chirp-corrected data in order to (i) filter noise out and (ii) drastically reduce the number of significant kinetic traces. The so-called orthogonal kinetic vectors associated to the seven largest singular values were simultaneously fitted to a sum of five exponentials, convoluted by a Gaussian function representing the instrument response function (IRF). The Gaussian function was typically found to have a full width at half maximum of 120 fs.

Two drawbacks of this procedure may be noted. Since the presence of XPM (see above) during pump-probe overlap could only be imperfectly taken into account by the best fitting functions known to us, we removed times below 0.2 ps from the final fit. The consequence is that some very fast molecular dynamics (with a time constant faster than about 50 fs) can be missed. It should also be noted that the present global analysis is formally not perfectly adapted to the treatment of continuously shifting bands. It indeed assumes that to a given exponential component corresponds a constant spectrum. The case of spectrally shifting bands is however correctly taken into account in practice by a single component taking the initial spectrum to the shifted spectrum.

The results are provided as a list of time constants associated to their pre-exponential factors at each wavelength, called decay-associated difference spectra (DADS). The global kinetics can then be conveniently summarized by formally assuming a cascading scheme (which does not mean that the actual reaction necessarily follows such a model), as follows:

$$|1\rangle \overset{\tau_1}{\rightarrow} |2\rangle \overset{\tau_2}{\rightarrow} \ldots |n\rangle \overset{\tau_n}{\rightarrow} |0\rangle$$

The initially excited state, noted $|1\rangle$, evolves to state $|2\rangle$, with time constant τ_1 and quantum yield 1. State $|2\rangle$ then gives state $|3\rangle$, with time constant τ_2 and quantum yield 1, and so on

until the initial ground state $|0\rangle$ is restored. The spectra associated to states $|i\rangle$ are called evolution-associated difference spectra (EADS). It should be noted that EADS1 is the initial spectrum extrapolated at time t = 0. Since it is deconvoluted from the instrument response function (IRF) and therefore relies very much on the quality of the IRF and on the procedure used to get rid of the XPM artifact, it should be taken with caution.

5.2. Free ligand

The whole set of transient absorption spectra of L (Fig. S22) was globally fitted to a sum of five exponentials, convoluted by the instrument response function. The average residue of the fit was 50×10^{-6} (OD units). The decay-associated difference spectra (DADS) are represented in Fig. S24.

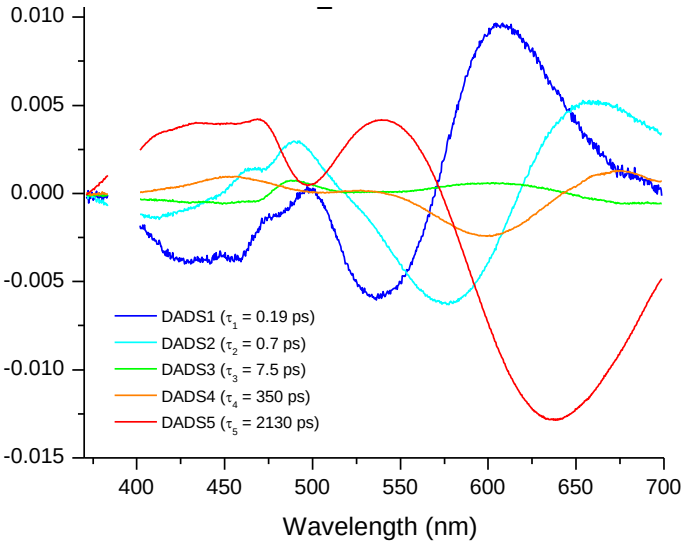

Figure S24. Global analysis of the transient absorption spectra of compound **9**: DADS of the free ligand L.

The corresponding EADS are shown in Fig. 2-left of the main text. The EADS1 of L is characterized by a negative stimulated emission (SE) band at 563 nm and a positive excited-state absorption (ESA) peak at 483 nm. It corresponds to the initially excited state, also called locally excited (LE) state, extrapolated at time t=0. It evolves in 190 fs to produce a new spectrum (EADS2), with ESA maxima at 470 and 530 nm and a SE band situated around 610 nm. According to previous studies on DCM and DCM-crown in solution,[4] the 530-nm band is characteristic of an emissive intramolecular charge transfer (ICT) state within the excited DCM moiety. EADS2 is further seen to evolve in 0.72 ps towards EADS3, with a red shift of the SE band (610 to 630 nm), a blue shift of the ESA band at 470 nm and a deepening of the

dip at 500 nm between the two ESA bands. This evolution, particularly the red shift of the SE band, can be interpreted by the dynamic solvation of the ICT state in acetonitrile, expected to occur with characteristic times of 0.089 (too fast to be observed here) and 0.63 ps.[5] During the third kinetic step (7.5 ps) only minor spectral changes are observed; the SE band of EADS3 in particular slightly shifts to the blue, by ~2 nm. A similar blue shift has been previously observed in a similar timescale for DCM in acetonitrile, and assigned to the cooling of the ICT state, initially formed with some excess vibrational energy.[4a] The spectral changes from EADS4 to EADS5 in 350 ps are more conspicuous. The most obvious one is a red shift of the SE emission band (from 628 to 637 nm), which is far too slow to be assigned to any solvation dynamics in acetonitrile. Such an effect was not previously observed for DCM[4a] or free DCM-crown in solution.[4c] We tentatively propose it to be due to a structural relaxation of the molecule, possibly involving the central calix[4]bis-crown scaffold (ether crowns and/or calixarene tube). Partial ground-state recovery likely accompanies this phase, as demonstrated by the decay of the ESA and SE bands. Finally EADS5, the spectrum of the long-lived excited state, decays to the ground state in 2.13 ns. Independent measurements performed on two different L samples yielded the same value of τ_5 within 0.05 ns.

5.3. ML90 sample

The transient absorption spectra of the ML90 sample were also globally fitted to a sum of five exponentials. The decay-associated difference spectra (DADS) are represented in Fig. S25.

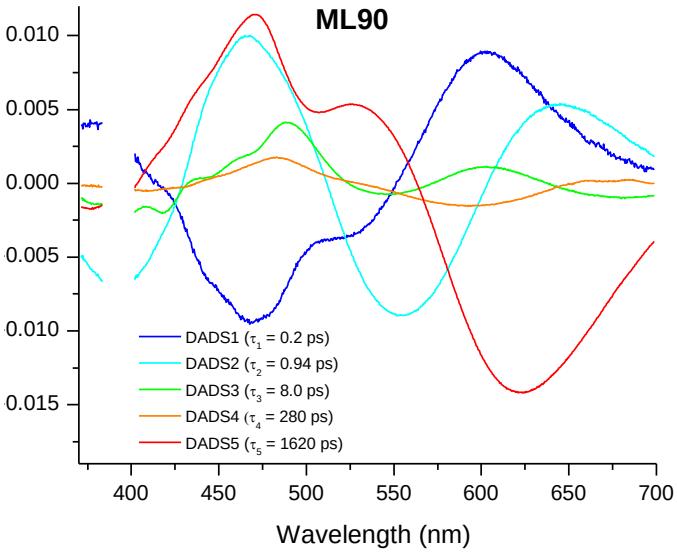

Figure S25. Global analysis of the transient absorption spectra of compound **9**: DADS of the ML90 sample.

Table S1 provides a comparison of the time constants obtained for L and ML90.

Table S1. Time constants of the 5-exponential global fitting obtained for L and ML90.

	L	**ML90**
τ_1 (ps)	0.19 ± 0.01	0.20 ± 0.01
τ_2 (ps)	0.7 ± 0.2	0.94 ± 0.2
τ_3 (ps)	7.5 ± 0.5	8.0 ± 0.3
τ_4 (ps)	350 ± 20	280 ± 30
τ_5 (ps)	2130 ± 30	1620 ± 20

The EADS of ML90 are shown in Fig. 2-right of the main text. EADS1 shows striking resemblance with that of L, with ESA at 473 nm and SE at 560 nm. A notable difference is seen in the negative ground-state bleaching (GSB) band, peaking at 420 nm for L and ~400 nm for ML90, but can be well explained by the absorption band of ML90 being strongly blue shifted compared to that of L. It thus appears that the EADS1 of ML90 should be assigned to the same LE state produced upon excitation of L. This conclusion means that metal-ligand interaction is extremely quickly disrupted upon excitation of ML_{DCM} and already complete in EADS1 (ML90). It is then interesting to note that the transient spectra of ML_{DCM} evolve similarly as those of L but more slowly. We observe in both cases the rise of the same ESA band at 530 nm, assigned to the ICT state of the (uncomplexed) DCM moiety. The kinetics of formation of this ICT state is however different. For L, the ICT state mostly appears with a time constant of 0.19 ps, then relaxes in 0.7 ps. For ML_{DCM} the process extends over a longer time, involving the first three time constants (0.20, 0.94 and 8.0 ps). Most of the ICT formation in fact takes place in 0.94 ps. We conclude that the presence of the K^+ ion in the vicinity of the N atom of the DCM anilino group substantially reduces the rate of the formation of the ICT state. The same observation was repeatedly made in the case of DCM-crown complexed to several metal ions (Li^+, Ca^{2+}, Sr^{2+})[4c,6] and it was proposed that the formation of the ICT is coupled to a movement of the cation away from the N atom of the crown, which lowers the potential energy barrier between LE and ICT states. The same interpretation may be used in the present case (ML_{DCM}). Like in the case of L, the first two time constants likely include the contribution of dynamic solvation from acetonitrile, as evidenced by the red shift of the SE band (Fig. 2-right). EADS4 also exhibits a slight blue shift of the SE band compared to EADS3 and the occurrence of a cooling phase of the newly formed ICT state may be invoked. From EADS4 to EADS5, the intensity of all bands is seen

to decrease, with a time constant of 280 ps, and a red shift (~3 nm) is observed in the SE band. This kinetic step is similar to the one reported for L (τ_4 = 350 ps), but exhibits a smaller shift (~9 nm for L). The same interpretation, namely the existence of structural relaxation involving the calixarene tube, may tentatively be proposed. The excited state characterized by EADS5 finally decays to the ground state with a time constant of 1.62 ns. Independent measurements performed on two different ML90 samples yielded the same value of τ_5 within 0.030 ns. The difference of τ_5 between L (2.13 ns) and ML_{DCM} (1.62 ns) must therefore be considered significant.

6. Shift dynamics of the SE band

6.1. Method

As explained in §5.1, the global analysis method used for fitting the transient absorption spectra of L and ML_{DCM} is not very well suited for describing the evolution of shifting bands, like the stimulated emission band of the present data. For this we used a more precise method: we extracted the frequency of the minimum of the SE band, by locally fitting the SE band with the sum of two lognormal functions and plotted it as a function of time. Fig. 3 (main text) displays the results. The starting time was chosen to be 0.2 ps in order to avoid the complex time region of pump-probe overlap. The obtained curve was in turn fitted by the sum of four exponential functions, the parameters of which are gathered in Table S2.

Table S2. Fit parameters for the SE band frequency shift curves, corresponding to the fitting function:
$\nu_{SE} = \nu_\infty + A_1 \exp(-t/\tau_{1s}) + A_2 \exp(-t/\tau_{2s}) + A_3 \exp(-t/\tau_{3s}) + A_4 \exp(-t/\tau_{4s})$

	L	**ML90**
ν_∞ (cm^{-1})	15623 ± 7	15650 ± 80
A_1 (cm^{-1})	-600 ± 800	620 ± 20
τ_{1s} (ps)	0.07 ± 0.04	0.22 ± 0.01
A_2 (cm^{-1})	620 ± 20	480 ± 20
τ_{2s} (ps)	0.80 ± 0.04	1.09 ± 0.05
A_3 (cm^{-1})	-60 ± 10	-114 ± 7
τ_{3s} (ps)	6 ± 2	6.2 ± 0.4
A_4 (cm^{-1})	293 ± 6	480 ± 80
τ_{4s} (ps)	630 ± 30	4000 ± 800

We recall that the SE band is in fact a superposition of pure stimulated emission, transient absorption and bleaching contributions. However, since the stimulated emission contribution is largely dominant at the minimum, the shift of the SE band mostly reflects the shift of the underlying pure stimulated emission contribution—although it may appear slightly distorted due to the superposition effect.

6.2. Free ligand

For the free ligand, the time constants of the shift dynamics are mostly consistent with the ones of global analysis (except for τ_{1s}=0.07 ps, too short to be considered meaningful). The red shift (A_2=620 cm^{-1}) associated with the second time constant (τ_{2s}=0.80 ps) and the smaller blue shift (A_3=-60 cm^{-1}) observed next (τ_{3s}=6 ps) correspond to the solvation dynamics of the ICT state and its subsequent cooling. The final rather slow red shift (A_4=293 cm^{-1}; τ_{4s}=630 ps) may be attributed to the structural relaxation of the calixarene core.

6.3. ML90 sample

The SE shift curve of ML90 displays an initial biexponential red shift (A_1+A_2=1100 cm^{-1}; τ_{1s}=0.22 ps, τ_{2s}=1.09 ps) corresponding to the delayed growth of the ICT state and its simultaneous solvation. Like in L, τ_{3s}=6.2 ps corresponds to a blue shift (A_3=-114 cm^{-1}), assigned to the cooling of the ICT state. The final red shift (A_4=480 cm^{-1}) is observed in τ_{4s}=4 ns. A large error is attached to this time constant (significantly longer than our 1.5-ns observation window) but it can safely be claimed that it is much longer than the corresponding value of 630 ps found for L.

The particularly large value of τ_{4s} for ML90 suggests that, in this case, the K^+ ion has not diffused very far away from the excited DCM in the sub-ns regime. Had this occurred, the 630-ps shift component of L would have been observed. The K^+ ion therefore still plays an active role on the DCM dynamics while the molecule decays to its ground state.

7. DFT and TDDFT calculations

Density Functional Theory (DFT) and Time Dependent Density Functional Theory (TDDFT) calculations were carried out with Becke-3-Lee-Yang-Parr (B3LYP) exchange functional and 6-31G (d) basis set by using the Gaussian 09 package. There are mainly two conformations of

the compound **9**, *cis* and *trans* (Fig. S26). The '*trans*' form is energetically more stable than the '*cis*' form (by ~ -4.086 kcal/mol in gas phase). Further calculations were carried out with the '*trans*' form. K^+ ions can occupy at a time either one or two crown cavities of a single molecule. To verify this, we calculated the binding energy of K^+ ion after optimizing the K^+-complexes when K^+ ions are in either of two cavities or in both. Fig. S26 represents the optimized structures of K^+-complexes (calculations related to K^+ ions in both of the cavities of a molecule are still going on). Basis Set Superposition Errors (BSSE) were corrected by the counterpoise method while calculating the binding energy. The calculated binding energies (in the gas phase) are -72.47 kcal/mol (in the cavity near DMABN) and -69.5 kcal/mol (in the cavity near DCM) respectively. The two binding energies are very close and one would expect that the potassium ion can be complexed as easily on the DCM and DMABN sides of the molecule. As shown by UV-vis spectroscopy, the first ion is in fact preferentially complexed on the DCM side. The discrepancy between calculation and experiment might be due to limitations in our theoretical description of the interaction between K^+ and the N atom of the crowns, possibly because of the use of a too small basis set.

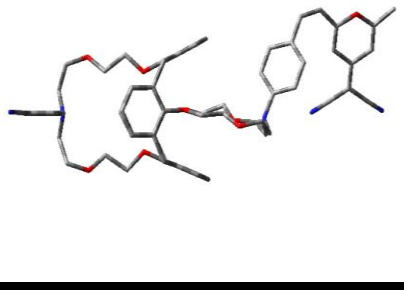

Optimized structure of compound **9** (cis)

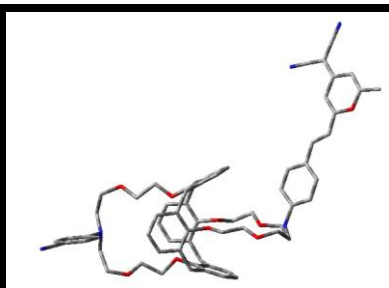

Optimized structure of compound **9** (trans)

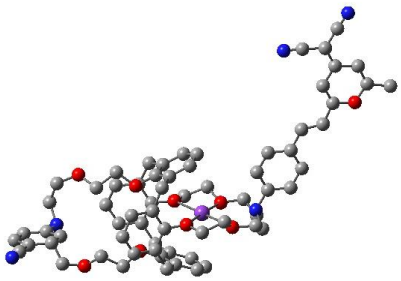

ML_{DCM} complex (K^+ near DCM part)

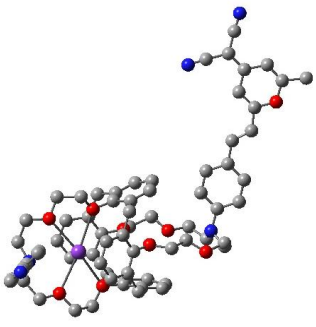

ML_{DMABN} complex (K^+ near DMABN part)

Figure S26. Optimized geometries of compound **9** ('*cis*' and '*trans*' form), K^+-complexes when K^+ ion occupies either of the two cavities, calculated at B3LYP/6-31G (d) level of theory. In molecular representation red, blue, grey and violet indicate respectively the oxygen, nitrogen, carbon and K^+ ion.

The absorption spectrum of compound **9** in acetonitrile shows that there are two major peaks around 298 nm and 468 nm and several bands in between them (Fig. 1A of the main text, black curve). Generally DMABN gives absorption peak around 290 nm and DCM gives major absorption peaks around 295 nm and 470 nm in highly polar solvents.[7] Therefore, peak around 295 nm may be generated from either DMABN or DCM moiety or from both while they are attached to the same scaffold. To get deeper insight into the origin of these characteristic bands, we carried out time dependent density functional theory (TDDFT) calculations and summarized the results in Table S3. The first singlet excited state (S_1) is associated with the longest wavelength (440 nm, calc.). Major contribution to this excited state comes from the HOMO→LUMO transition. HOMO and LUMO are located mainly in DCM moiety, which indicates that lowest energy band in the absorption spectrum of compound **9** originates from the DCM moiety. Similarly, it is noted that the peaks around 332 nm and 313 nm (corresponding to S_{12} and S_{14} excited states) also originate from the DCM moiety (Table S3 and Fig. S27). We could not calculate higher excited states beyond S_{15} because of the large molecular size of the current compound. So, we could not interpret precisely the origin of the peak around 300 nm.

The intensity of the two major peaks at 298 and 468 nm in the absorption spectrum decreases and intensity of the bands between these two peaks increases with increasing concentrations of K^+ ions (Fig. 1A of the main text, red curve). To rationalize this experimental observation at the molecular level we further carried out DFT and TDDFT calculations and summarized the results in Table S4 and Fig. S28. The occupation of K^+ ion into the crown cavity near DCM moiety reduces the electron density of the HOMO located at DCM moiety (cf. HOMO of compound **9** and HOMO of K^+-complex), which reduces the overlap integral between HOMO and LUMO electron density giving the lower oscillator strength (0.2766). On the other hand, presence of K^+ ion in the cavity restricts the electron density distribution of the HOMO-2 into the calixarene as well as crown ring (see HOMO-2 of compound **9** and HOMO-2 of K^+-complex), which, in turn, localize the electron density of HOMO-2 into DCM moiety and increases the overlap integral between HOMO-2 and LUMO (e.g. HOMO-

2→LUMO transition for S_{12} state) giving much higher oscillator strength (1.1346). These are consistent with the experimental observations.

Table S3. Main excitations and oscillator strengths corresponding to various singlet excited states in compound **9**. Excited states corresponding to higher oscillator strengths (>0.1) are only tabulated.

Excited States	Excitations	Oscillator Strength	Calc. λ_{max} (nm)	Expt. λ_{max} (nm)
S_1	HOMO→LUMO(69.3%)	0.8381	440	468
S_{12}	HOMO-2→LUMO(13.2%) HOMO →LUMO+1(54.1%)	0.1886	332	320-400
S_{14}	HOMO-12→LUMO (48.6%) HOMO-2 →LUMO+1(32.6%) HOMO-1 →LUMO+1(17.0%) HOMO→LUMO+1(33.8%)	0.3522	313	298

Table S4. Main excitations and oscillator strengths corresponding to various singlet excited states in compound **9** complexed with K^+. Excited states corresponding to higher oscillator strengths (>0.1) are only tabulated.

Excited States	Excitations	Oscillator Strength	Calc. λ_{max} (nm)	Expt. λ_{max} (nm)
S_1	HOMO→LUMO(68.6%)	0.2766	460	468
S_3	HOMO-2→LUMO(60.5%) HOMO →LUMO+1(12.7%) HOMO→LUMO 33.1%)	1.1346	333	400
S_{11}	HOMO→LUMO+1(40.3%) HOMO→LUMO+3(14.3%)	0.1903	313	298

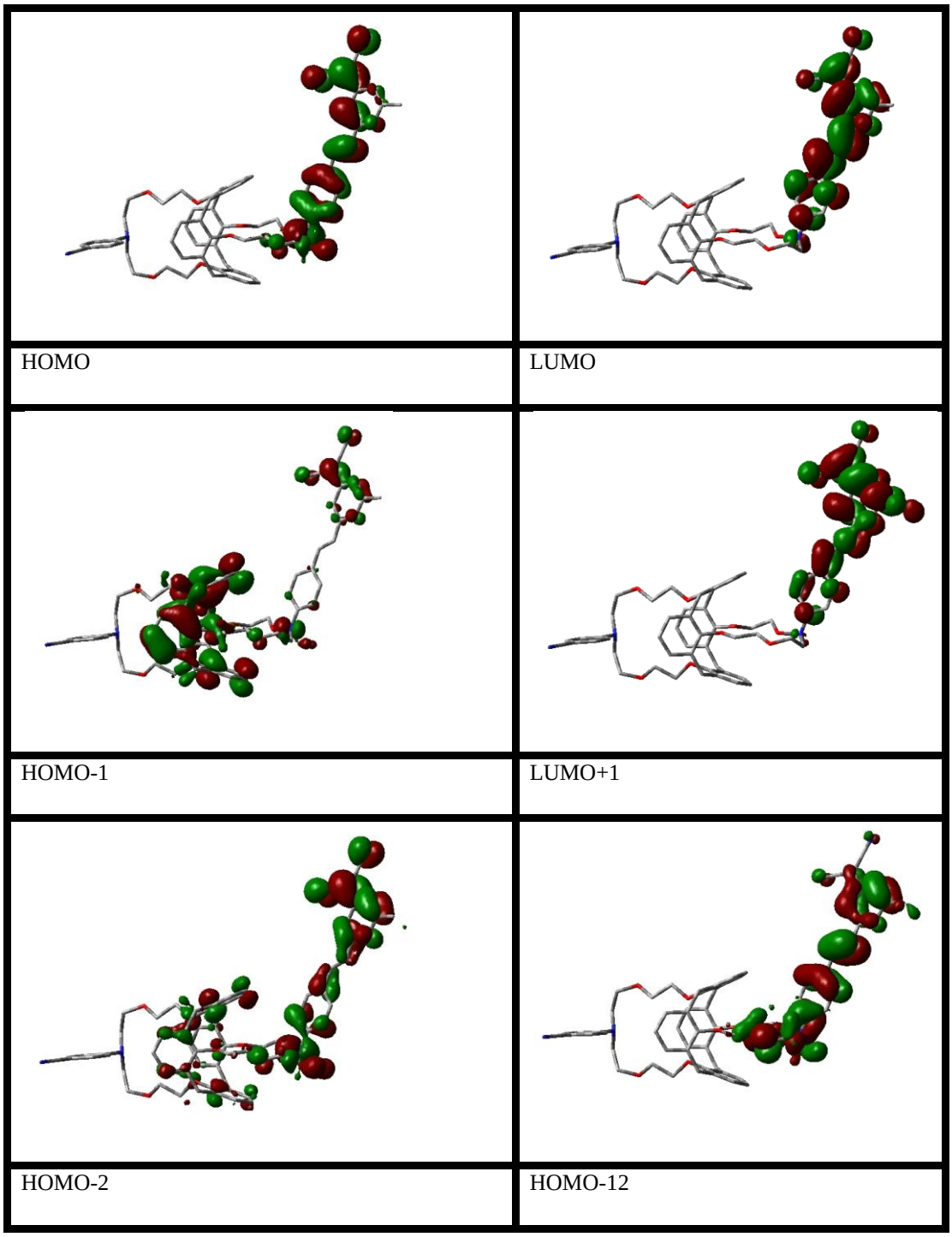

Figure S27. Profiles of frontier molecular orbitals of compound **9**. These MOs are involved in major transitions summarized in Table S3. Green and red correspond to the different phases of the molecular wave functions for the HOMOs and LUMOs, and the isovalue is 0.02 a.u.

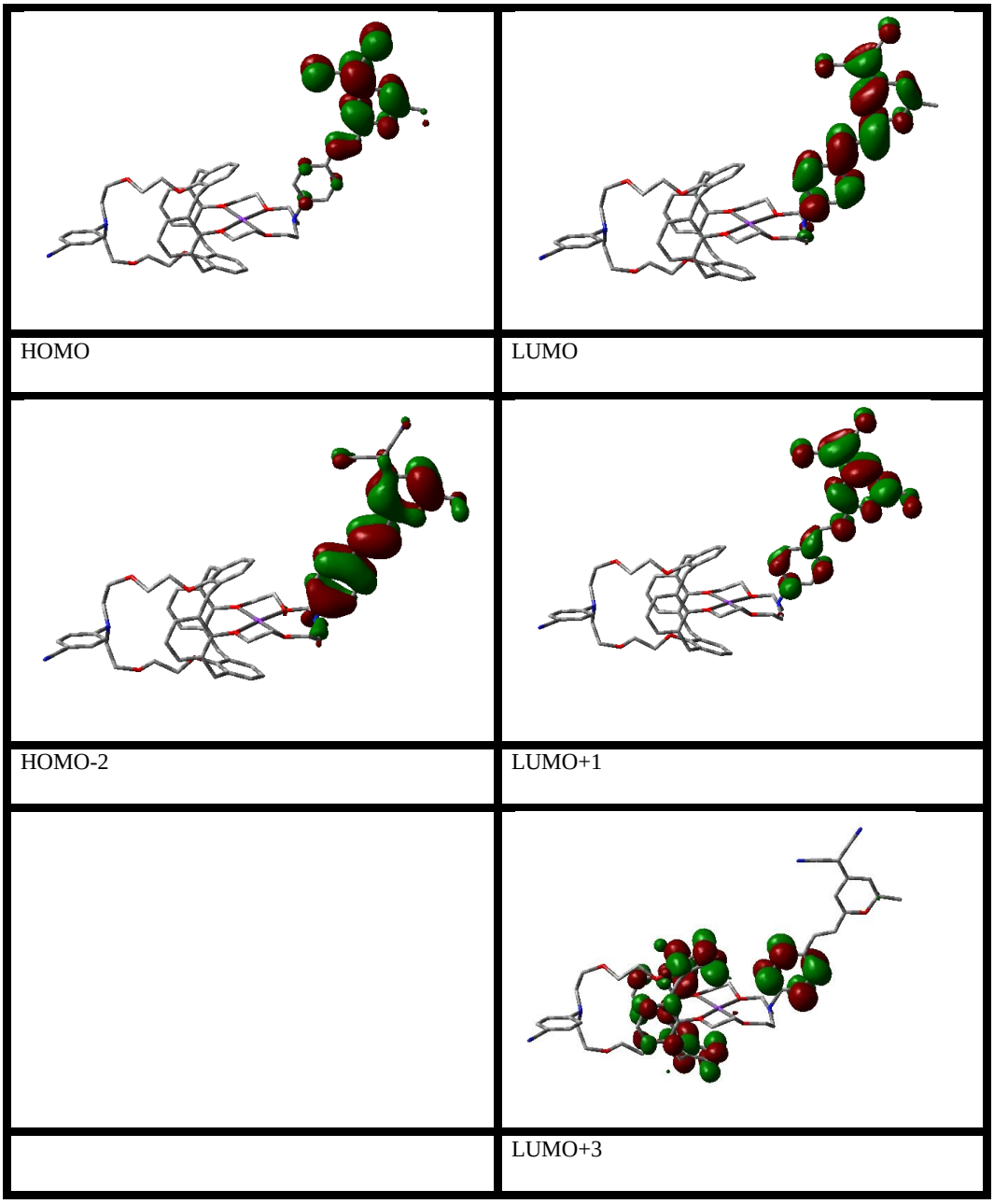

Figure S28. Profiles of frontier molecular orbital of K^+-complexes. These MOs are involved in major transitions summarized in Table S4. Green and red correspond to the different phases of the molecular wave functions for the HOMOs and LUMOs, and the isovalue is 0.02 a.u.

Supplementary References

1. B. Valeur, I. Leray, L. Zhao, V. Souchon, R. Metivier, P. Plaza, C. Ley, F. Lacombat and M. M. Martin, *ChemPhysChem*, 2010, **11**, 2416.
2. I. H. M. van Stokkum, D. S. Larsen and R. van Grondelle, *Biochim. Biophys. Acta Bioenerg.*, 2004, **1657**, 82.
3. E. R. Henry, J. Hofrichter and M. L. J. Ludwig Brand, in *Methods Enzymol.*, Academic Press, 1992, vol. 210, pp. 129.
4. (a) M. M. Martin, P. Plaza and Y. H. Meyer, *Chem. Phys.*, 1995, **192**, 367; (b) S. A. Kovalenko, N. P. Ernsting and J. Ruthmann, *Chem. Phys. Lett.*, 1996, **258**, 445; (c) M. M. Martin, P. Plaza, Y. H. Meyer, F. Badaoui, J. Bourson, J. P. Lefevre and B. Valeur, *J. Phys. Chem.*, 1996, **100**, 6879.
5. M. L. Horng, J. A. Gardecki, A. Papazyan and M. Maroncelli, *J. Phys. Chem.*, 1995, **99**, 17311.
6. (a) P. Plaza, I. Leray, P. Changenet-Barret, M. M. Martin and B. Valeur, *ChemPhysChem*, 2002, **3**, 668; (b) C. Ley, F. Lacombat, P. Plaza, M. M. Martin, I. Leray and B. Valeur, *ChemPhysChem*, 2009, **10**, 276.
7. M. Meyer and J. C. Mialocq, *Opt. Commun.*, 1987, **64**, 264.